

1 **An Early Miocene skeleton of *Brachydiceratherium* Lavocat, 1951 (Mammalia,**
2 **Perissodactyla) from the Baikal area, Russia, and a revised phylogeny of Eurasian**
3 **teleoceratines**

4 Alexander Sizov^{a, b}, Alexey Klementiev^b and Pierre-Olivier Antoine^c

5

6 a. Geological Institute of Russian Academy of Science, Pyzhevskii pereulok, 7, bld., 1,
7 Moscow 119017, Russia

8 b. Institute of the Earth's Crust of the Russian Academy of Sciences, Siberian Branch,
9 Lermontova St., 128, Irkutsk, 664033, Russia.

10 c. Institut des Sciences de l'Evolution, UMR 5554 Univ Montpellier, CNRS, IRD, Place
11 Eugène Bataillon, 34095 Montpellier cedex 5, France

12

13 **Abstract.** Hippo-like rhinocerotids, or teleoceratines, were a conspicuous component of
14 Holarctic Miocene mammalian faunas, but their phylogenetic relationships **remain poorly**
15 **known**. Excavations in lower Miocene deposits of the Olkhon Island (Tagay locality, Eastern
16 Siberia; 16–18 Ma) have opened a unique window on the poorly-known early history of the
17 Lake Baikal ecosystems, notably **by** unearthing a skeleton of the teleoceratine
18 *Brachydiceratherium shanwangense* (Wang, 1965). **The remains** provide new insights into the
19 **skull** and postcranial **morphology** of this elusive species. **The new material is compared with**
20 **other Eurasian teleoceratines and the relationships within Teleoceratina are investigated**
21 **through a phylogenetic analysis**. *Diaceratherium* Dietrich, 1931 (earliest Miocene, Western
22 Europe) **is found to be monotypic and is** retrieved as the earliest teleoceratine offshoot. Other
23 genera **have more than one species and are also found to be** monophyletic, with
24 *Prosantorhinus* Heissig, 1974 (early Miocene, Eurasia) **+** *Teleoceras* Hatcher, 1894
25 (Miocene, North America) forming the sister clade of *Brachypotherium* Roger, 1904

26 (Miocene, Old World) + *Brachydiceratherium* Lavocat, 1951). *Brachydiceratherium* includes
27 eight species spanning the late Oligocene to Late Miocene in Europe and Asia. All
28 teleoceratine genera except *Diaceratherium* span considerable geographical and
29 stratigraphical ranges, likely related to their ultra-generalist ecological preferences.
30
31 **Keywords:** Rhinocerotidae, *Brachydiceratherium shanwangense*, Tagay, Early Miocene,
32 Siberia, Lake Baikal, phylogeny, biogeographical history.

33 INTRODUCTION

34 Although they are nearly extinct today, rhinocerotids were one of the most widespread
35 and successful groups of large mammals on all the northern continents for over 40 million
36 years. They have occurred across Eurasia and North America since middle Eocene times, and
37 are known from Africa since the Early Miocene (e.g., Prothero et al., 1989; Antoine et al.,
38 2003, accepted; Geraads, 2010). They have also occupied many different locomotory modes,
39 ranging from slender- and long-legged savannah roamers (e.g., elasmotheriines) to hippo-like
40 forms that apparently lived along rivers and lakes (teleoceratines; Prothero et al., 1989;
41 Antoine, 2002). Most hippo-like rhinocerotids are gathered within teleoceratines, a clade at
42 the tribal to sub-tribal level, the phylogenetic relationships of which have never been fully
43 elucidated (Antoine, 2002; Lu et al., 2021). Most teleoceratines had skulls that were either
44 hornless or with a small nasal horn, barrel-shaped bodies, and shortened limb bones.
45 Teleoceratines span the late Oligocene–latest Miocene in Eurasia (Antoine, in press), the
46 Miocene in Africa (Geraads & Miller, 2013), and the early Miocene–early Pliocene in North
47 and Central America (Prothero, 2005). Most of them are interpreted to have been browsers
48 (based on both dental morphology and isotopic studies; MacFadden, 1998; Hullot et al.,
49 2021).

50 In this study, we describe a skeleton of a teleoceratine from Lower Miocene deposits of
51 Olkhon Island, Lake Baikal area, Siberia. We identify its species assignment and compare it
52 to most teleoceratine species described from Eurasia. This in-depth comparison forms the
53 basis for performing a parsimony analysis of phylogenetic relationships among Eurasian
54 Teleoceratina, and for discussing key events in the paleobiogeography of teleoceratine
55 rhinocerotids.

56 LOCALITY AND GEOLOGICAL SETTINGS

57 Lake Baikal, located in the Baikal Rift System, is morphologically characterised by
58 three basins (Southern, Central and Northern). The Southern and Central basins are thought to
59 have existed permanently since the Paleogene, whereas the Northern Basin did not develop
60 before the Late Miocene (Mats et al., 2010, 2011). Olkhon Island (Russian: ОЛЬХОН) is
61 located in the transitional zone between the Central and the Northern basins of Lake Baikal. It
62 is separated from the mainland in the west by a shallow Maloe More strait (Russian: Малое
63 Море; in English literally the Small Sea) of the Northern Basin that extends far to the south.
64 In the south, Maloe More strait is connected through the narrow Olkhonskie Vorota strait
65 (Russian: ОЛЬХОНСКИЕ ВОРОТА; in English literally the Olkhon Gate) to the central part of
66 Lake Baikal. From the northwestern part of Olkhon Island, one locality known as Tagay or
67 Tagai (Russian: Тарай or Торай) has yielded numerous terrestrial fossils of the Neogene (Fig.
68 1). The Neogene sediments in Tagay Bay belong to the Tagay Formation (Logachev et al.,
69 1964; Mats et al., 2001; Mats, 2013, 2015). Sediments are exposed in the northeastern part of
70 the bay in a steep erosional cliff up to 15 m high. Elsewhere along the shores of the bay, this
71 cliff is levelled by landslides. The cliff borders a large landslide cirque and a sandy beach
72 below.

73 The Tagay locality was discovered in the 1950s (Kitainik & Ivaniev, 1958). The first
74 paleontological studies of the large mammals were performed in 1958 under the direction of
75 N.A. Logachev (Logachev et al., 1964). Studies of small mammals have been carried out
76 since the 1970s (Pokatilov, 2004; Daxner-Höck et al., 2022). Tagay preserves an abundant
77 fossil fauna that includes molluscs and vertebrates such as fish, amphibians, reptiles, birds and
78 mammals. However, a significant part of the paleontological material was determined for the
79 longest time only tentatively: Mustelidae and Felidae among carnivorans, *Anchitherium* sp.,
80 *Metaschizotherium*(?) sp., and *Dicerorhinus*(?) sp. among perissodactyls, *Palaeomeryx* sp.
81 and Bovidae indet. among artiodactyls (Logachev et al., 1964). The reexamination of
82 artiodactyl remains led to the identification of Cervidae (*Amphitragulus boulangeri*,
83 *Lagomeryx parvulus*, *Stephanocemas* sp.), Palaeomerycidae (*Orygotherium tagaiense*,
84 *Palaeomeryx* cf. *kaupi*) and Anthracotheriidae (*Brachyodus intermedius*) (Vislobokova, 1990,
85 1994, 2004). Chelonians were studied by Khosatzky and Chkhikvadze (1993) and the
86 ichthyofauna by Filippov & Sytchevskaya (2000).

87 Small mammals from the Tagay-1 section were recently revised, with a list of 21 taxa
88 documenting erinaceids, talpids, plesiosoricids, and soricids among eulipotyphlans,
89 palaeolagid lagomorphs, and sciurids, aplodontids, mylagaulids, glirids, castorids, eomyids,
90 and cricetodontine muroids among rodents (Daxner-Höck et al., 2022).

91 The sedimentological, stratigraphical, and palaeontological aspects of the sediments were
92 described by Kossler (2003). A new phase of the study of Tagay locality started in 2008, with
93 numerous publications since that time (Rage & Danilov, 2008; Klementiev, 2009; Danilov et
94 al., 2012; Syromyatnikova, 2014, 2015; Tesakov & Lopatin, 2015; Klementiev & Sizov,
95 2015; Zelenkov, 2016; Sotnikova et al, 2021).

96 The Tagay Formation consists of alternating beds of clays and clayey sands containing
97 interlayers and lenses of carbonate concretions of diagenetic origin. Deposits rest upon the

98 crystalline basement, and are submerged below water to the south. Clay beds are mostly green
99 and brown, sometimes black. There are also lenses and interlayers of brick red and red clay
100 and loam. Bone beds, deposited in successive sedimentary cycles, were given letters from top
101 to bottom (i.e., downsection: A–H; Fig. 2 A, B). Most clay beds have predominant
102 ferruginous-magnesian montmorillonites composition. A remarkable feature of these clay
103 sediments is the high (up to 8%) content of silt-psammite-psephite admixtures. Moreover,
104 most psammite-psephitic fragments are not rounded and have angular and indented outlines,
105 which indicates a lack of transportation. The lithology of the sections and further details on
106 the bone beds were described in other studies (Logachev et al., 1964; Sizov & Klementiev,
107 2015).

108 Neogene continental deposits in the late early Miocene Tagay locality have yielded a
109 diverse vertebrate fauna. Following most works, the age of the Tagay Fauna correlates to the
110 European Mammal Zones MN3 through MN5 (20–15 Ma; Rössner & Mörs, 2001;
111 Vislobokova, 2004; Klementiev & Sizov, 2015; Sotnikova et al., 2021). Other researchers
112 have correlated the Tagay fauna or to MN 7+8 and Chinese Mammal Unit NMU7 (13–11 Ma;
113 Daxner-Höck et al., 2013). More recently, Daxner-Höck et al. (2022) proposed a more precise
114 age of ~16.5-16.3 Ma based on micromammalian biostratigraphy and the magnetic polarity
115 pattern of the Tagay-1 section (Fig. 1 B), which is in agreement with our preferred interval.

116 MATERIAL AND METHODS

117 All the remains described here belong to a single adult individual (IZK79-1-08C-1/),
118 stored in the collection of the Institute of the Earth's Crust (Irkutsk, Russia). Alexey
119 Klementiev and Gennady Turkin discovered this skeleton in 2008 at Tagay (Fig. 2 B, C)
120 (Klementiev, 2009).

121 Capital letters are used for upper teeth (I, C, D, P, M), and lower-case letters for lower teeth
122 (i, c, d, p, m). Rhinocerotid dental terminology follows Heissig (1969, 1972a: pl. 13) and
123 Antoine (2002), while dental and skeletal measurements were taken according to Guérin
124 (1980). Anatomical **descriptions** follow basically the same sequence as in Antoine (2002), and
125 Antoine et al. (2010). Dimensions are given in mm.

126 The stratigraphical framework is based on the **Neogene geological time scale** and
127 European Land Mammal Ages (Hilgen, Lourense & Van Dam, 2012; Raffi et al, 2020).

128 **3D-rendering**

129 All bones of the rhinoceros were scanned with a resolution of 0.25 mm using a
130 RangeVision Smart **3D scanner**. RangeVision Smart has three areas of scanning and is
131 equipped with colour cameras 1.3 **megapixels. We used the associated RangeVision 2020.2**
132 **software** for visualization, segmentation and 3D rendering.

133 **Phylogenetic analysis**

134 The **phylogenetic** analysis was **based on** 282 cranio-mandibular, dental, and postcranial
135 characters primarily derived from **the dataset** of Antoine (2002, 2003) **which was** scored on 31
136 ceratomorph species (one tapirid **and** 30 rhinocerotoids). All multistate characters were
137 treated as additive, except for the characters 72, 94, 102, 140, 187, **and 269** (non-additive; as
138 in Antoine, 2002).

139 The living Brazilian tapir *Tapirus terrestris* (Linnaeus, 1758), the Eocene non-
140 rhinocerotid rhinocerotoid *Hyrachyus eximius* Leidy, 1871 and the Paleogene stem
141 rhinocerotids *Trigonias osborni* Lucas, 1900 (Eocene of North America) and *Ronzotherium*
142 *filholi* (Osborn, 1900) (Oligocene of Western Europe) **were selected as outgroups. We** also
143 included a branching group (Antoine, 2002, 2003; Orliac et al., 2010; Boivin et al., 2019),
144 **consisting of non-teleoceratine taxa, with the aim of testing the monophyly and relationships**

145 of the Teleoceratina among the Rhinocerotinae. These consist of 12 species, including an
146 early-diverging representative of Rhinocerotinae (*Plesiaceratherium mirallesi* (Crusafont,
147 Villalta & Truyols, 1955)), three species of Aceratheriini (*Aceratherium incisivum* Kaup,
148 1832, *Acerorhinus zernowi* (Borissiak, 1914), and *Alicornops simorreense* (Lartet, 1851)), and
149 eight members of the Rhinocerotina, encompassing all five living rhinoceroses, namely the
150 Indian rhino (*Rhinoceros unicornis* Linnaeus, 1758), the Javan rhino (*Rhinoceros sondaicus*
151 Desmarest, 1822), the Sumatran rhino (*Dicerorhinus sumatrensis* (Fischer, 1814)), the white
152 rhino (*Ceratotherium simum* (Burchell, 1817)), and the black rhino (*Diceros bicornis*
153 (Linnaeus, 1758)), in addition to three fossil species: *Lartetotherium sansaniense* (Lartet in
154 Laurillard, 1848) (Miocene of Europe; Heissig, 2012), *Gaindatherium browni* Colbert, 1934
155 (Miocene of South Asia; Heissig, 1972a; Antoine, in press), and *Nesorhinus philippinensis*
156 (Von Koenigswald, 1956) (early Middle Pleistocene of the Philippines; Antoine et al., 2022
157 and references therein).

158 The ingroup sensu stricto (Teleoceratina) comprises 15 taxa, with *Teleoceras fossiger*
159 Cope, 1878 (late Miocene to earliest Pliocene, North America), *Brachypotherium brachypus*
160 (Lartet in Laurillard, 1848) (late early and middle Miocene, Eurasia), *Brachypotherium*
161 *perimense* (Falconer & Cautley, 1847) (Miocene, South Asia), *Prosantorhinus germanicus*
162 (Wang, 1929) (late early and middle Miocene, Europe), *Prosantorhinus douvillei* (Osborn,
163 1900) (late early and early middle Miocene, Europe), *Prosantorhinus laubei* Heissig & Fejfar,
164 2007 (early Miocene, central Europe), and a comprehensive sample of taxa either classically
165 or more recently assigned to *Diaceratherium* Dietrich, 1931. These consist of the type species
166 *D. tomerdingense* Dietrich, 1931 from the earliest Miocene of Tomerdingen (Germany), *D.*
167 *lemanense* (Pomel, 1853) from the latest Oligocene-early Miocene of Western Europe (also
168 described under the *Diceratherium* (*Brachydiceratherium*) *lemanense* combination by
169 Lavocat, 1951), *D. aurelianense* (Nouel, 1866) from the early Miocene of Western Europe.

170 The taxonomic sample also includes *D. asphaltense* (Depéret & Douxami, 1902) from the
171 earliest Miocene of Western Europe, *D. fatehjangense* (Pilgrim, 1910), from the Miocene of
172 Pakistan and early Miocene of Kazakhstan (previously described as “*Brachypotherium*
173 *aurelianense* Nouel, var. nov. *Gailiti*” by Borissiak, 1927), and *D. aginense* (Répelin, 1917)
174 from the earliest Miocene of Western Europe. Lastly, we have considered *D. shanwangense*
175 (Wang, 1965) from the late early Miocene of eastern China (Shanwang; Lu et al., 2021),
176 Japan, and eastern Siberia (Tagay; this work), and *D. lamilloquense* Michel, in Brunet et al.,
177 1987 from the late Oligocene of France. We also included *Aceratherium gajense intermedium*
178 Lydekker, 1884, which has disputed taxonomic affinities. It was previously assigned to the
179 aceratheriine genera *Subchilotherium* (e.g., Heissig, 1972a) or *Chilotherium* (e.g., Khan et al.,
180 2011), although based on a parsimony analysis taking into account the holotype and original
181 hypodigm, Antoine et al. (2003) considered that it might be a teleoceratine instead, of
182 uncertain generic assignment. The recognition of associated dental and postcranial remains
183 from the Potwar Plateau (late early to early late Miocene, Pakistan) allowed for defining the
184 new combination *Diaceratherium intermedium* (Lydekker, 1884) for this taxon, as recently
185 proposed by Antoine (in press).

186 Three representatives of Teleoceratina, *Diaceratherium* cf. *lamilloquense* from the late
187 Oligocene of Thailand (Marivaux et al., 2004), *Brachypotherium gajense* (Pilgrim, 1910),
188 from the late Oligocene–earliest Miocene of Pakistan, and *Prosantorhinus shahbazi* (Pilgrim,
189 1910), from the early Miocene of Pakistan (combinations proposed by Antoine et al., 2010
190 and Antoine, in press) were not included in the analysis, due to their poorly-known
191 hypodigms, restricted to a few elements.

192 Moreover, *Diaceratherium askazansorense* Kordikova, 2001 from the early Miocene of
193 Kazakhstan was not included, as dental and postcranial elements assigned to this taxon
194 closely resemble those of *Pleuroceros blanfordi*, a stem member of Rhinocerotinae (early

195 Miocene of South Asia; Antoine et al., 2010; Prieto et al., 2018) and, to a lesser extent, of
196 *Pleuroceros pleuroceros* (earliest Miocene of western Europe; Antoine et al., 2010; Antoine
197 & Becker, 2013). Similarly, the early late Oligocene species *Diaceratherium massiliae*
198 Ménouret & Guérin, 2009 was recently shown to be a junior synonym of the short-limbed and
199 early-diverging rhinocerotid *Ronzotherium romani* Kretzoi, 1940, through a re-examination of
200 most available material and the recognition of new associated dental and postcranial
201 specimens in Switzerland (Tissier et al., 2021).

202 Details on the specimens, collections, direct observation and/or literature used for
203 scoring taxa, with references used) are provided as taxon notes in the morphological data
204 matrix (supplementary file S3).

205 The parsimony analyses were performed through the heuristic search of PAUP 4 3.99.169.0
206 (Swofford, 2002), with tree-bisection-reconnection (reconnection limit = 8), 1000 replications
207 with random addition sequence (10 trees held at each step), gaps treated as missing, and no
208 differential weighting or topological constraints. Branch support was estimated through
209 Bremer indices (Bremer, 1994), also calculated in PAUP 4 3.99.169.0.

210 Systematics

211 Generic and suprageneric systematics follow the present parsimony analysis (see
212 below).

213 SYSTEMATIC PALAEOLOGY

214 Order Perissodactyla OWEN, 1848

215 Family Rhinocerotidae GRAY, 1821

216 Subfamily Rhinocerotinae GRAY, 1821

217 Tribe Rhinocerotini GRAY, 1821

218 Subtribe Teleoceratina HAY, 1902

219 Genus *Brachydiceratherium* LAVOCAT, 1951
220 Syn. *Diaceratherium* DIETRICH, 1931 (partim)

221

222 **Type species:** *Acerotherium lemanense* Pomel, 1853 by subsequent designation
223 (Lavocat, 1951)

224

225 **Included species:** *Rhinoceros aurelianensis* Nouel, 1866 from the early Miocene of
226 Western Europe; *Aceratherium intermedium* Lydekker, 1884, from the early–late Miocene of
227 the Indian Subcontinent and China (Deng and Gao, 2006; Antoine et al., 2013; Antoine, in
228 press); *Diceratherium asphaltense* Depéret & Douxami, 1902 from the earliest Miocene of
229 Western Europe; *Teleoceras fatehjangense* Pilgrim, 1910, from the Miocene of Pakistan and
230 early Miocene of Kazakhstan (senior synonym of “*Brachypotherium aurelianense* Nouel, var.
231 nov. *Gailiti*” by Borissiak, 1927); *Teleoceras aginense* Répelin, 1917 from the earliest
232 Miocene of Western Europe; *Plesiaceratherium shanwangense* Wang, 1965 from the late
233 early Miocene of eastern China (Shanwang; Lu et al., 2021), Japan, and eastern Siberia
234 (Tagay; this work); *Diaceratherium lamilloquense* Michel, in Brunet et al., 1987 from the late
235 Oligocene of France.

236

237 **Diagnosis:** Teleoceratines with a small nuchal tubercle, articular tubercle smooth on the
238 squamosal, with cement present on cheek teeth, protocone always constricted on P3-4, labial
239 cingulum usually absent on lower premolars and always present on lower molars, foramen
240 vertebrale lateralis present and axis-facets transversally concave on the atlas, a postero-distal
241 apophysis low on the tibia, and a latero-distal gutter located posteriorly on the fibula.

242 Distinct from *Diaceratherium tomerdingense* in possessing a long metaloph on M1-2,
243 no mesostyle on M2, a distal gutter on the humeral epicondyle, an anterior side of the

244 semilunate with a sharp distal border, no posterior expansion on the pyramidal-facet of the
245 unciform, and a trapezium-facet present on the McII.

246 Differs from representatives of *Brachypotherium* in having close parietal crests, a
247 median ridge on the occipital condyles, a mandibular symphysis less massive, a labial
248 cingulum usually or always absent on upper premolars, an external groove developed on the
249 ectolophid of lower cheek teeth, a V-shaped lingual opening of the posterior valley of lower
250 premolars (in lingual view), a paraconid developed on p2, no second distal radius-ulna facet, a
251 symmetric semilunate-pyramidal distal facet, a posterior McIII-facet present on the McII, and
252 a fibula-facet subvertical on the astragalus.

253 Distinct from species referred to as *Prosantorhinus* in showing no latero-ventral
254 apophysis on the nasals, close fronto-parietal crests, and no posterior groove on the processus
255 zygomaticus of the squamosal.

256

257 **Geographical and stratigraphical range:** Late Oligocene and Miocene of Eurasia,
258 with an Early Miocene climax.

259

260 *Brachydiceratherium shanwangense* (Wang, 1965)

261 See synonymy list in Lu et al. (2021)

262

263 **Holotype:** IVPP V 3026, left maxilla with upper cheek tooth series (P2-M3), stored at
264 the Institute of Vertebrate Paleontology and Paleoanthropology, Chinese Academy of
265 Sciences (IVPP).

266

267 **Stratum typicum and locus typicus:** Early Miocene (Shanwang Formation,
268 Shanwangian Age/Stage of China, middle Burdigalian); Xiejiahe locality, Shanwang Basin,
269 Shandong, China (see Lu et al., 2021).

270

271 **Diagnosis:** Representative of *Brachydiceratherium* with a lateral apophysis present on
272 the nasals, a median nasal horn present on the nasals, premolar series short with respect to the
273 molar series, roots distinct on the cheek teeth, crochet always simple and lingual cingulum
274 usually absent and always reduced on P2-4, crista always present on P3, protocone strongly
275 constricted on M1-2, lingual cingulum usually absent on lower premolars and always absent
276 on lower molars, d1/p1 absent in adults, glenoid fossa with a medial border straight on the
277 scapula, distal gutter absent on the lateral epicondyle of the humerus, proximal radius-ulna
278 facets always fused, and trochanter major low on the femur.

279 Distinguished from *Bd. lamilloquense*, *Bd. lemanense*, *Bd. asphaltense*, and/or *Bd.*
280 *aurelianense* in having I1s oval in cross section, no labial cingulum on upper cheek teeth, a
281 strong paracone fold on M1-2 and a constricted hypocone on M1, M3s with a triangular
282 occlusal outline, a radius with a high posterior expansion of the scaphoid-facet, a femoral
283 head hemispheric, an astragalus with a laterodistal expansion, very low-and-smooth
284 intermediate reliefs on metapodials, and a long insertion of m. interossei on lateral
285 metapodials.

286 Differs from *Bd. aginense* in having a processus postorbitalis on the frontal bone and a
287 median ridge on the occipital condyle, but no posterior groove on the processus zygomaticus
288 of the squamosal, molariform P2s (protocone and hypocone lingually separate), a long
289 metaloph on M1-2, a posterior groove on M3, a shallow gutter for the m. extensor carpi on the
290 radius, a posterior MtII- MtIII facet developed, but no cuboid-MtIII contact.

291 Distinct from *D. intermedium* in showing usually a lingual cingulum on upper molars, a
292 strong paracone fold on M1-2, a lingual cingulum usually absent on lower premolars, and a
293 right angle between the cuboid-facet and the base of the tuber calcanei on the calcaneus
294 Differs from *Bd. lemanense* in possessing a low zygomatic arch with a processus postorbitalis,
295 a small processus posttympanicus and a well-developed processus paraoccipitalis.
296 Distinct from *Bd. asphaltense* in having closer fronto-parietal crests and a brachycephalic
297 shape.
298 Differs from *D. lamilloquense* in showing a protoloph joined to the ectoloph on P2 and
299 molariform P3-4s (protocone and hypocone lingually separate).
300 Differs from *D. aurelianense* in having no metaloph constriction on P2-4 and a protocone
301 weakly developed on P2.

302

303 **Geographical and stratigraphical range:** Late early Miocene of the Shanwang Basin,
304 Shandong Province, China (see Lu et al., 2021) and of Irkutsk Region, Russia (Tagay locality,
305 Olkhon Island, Lake Baikal).

306

307 **Material studied:** IZK79-1-08C-1, almost complete skeleton, including the skull
308 (occipital, parietal, frontal, the right zygomatic and lacrimal, both nasals, and temporals with
309 processes and also premaxillae), the jaws, most vertebrae and ribs, both humeri, radii and
310 ulnae, both femora, tibiae, right fibula, most metacarpals, and several metatarsals and
311 phalanges. The skeleton described herein was found disarticulated at the junction of layers of
312 sand and clay (Fig. 2 B, C). In general, the right side of the individual is much better
313 preserved than the left one.

314 DESCRIPTION

315 **Skull**

316 The skull (Fig. 3, Table 1) was found disarticulated, but there is no doubt that the
317 separate bones belong to the same individual, because they were found in close proximity to
318 one another with no extraneous elements, and they fit together well. The temporal, zygomatic
319 and lacrimal, nasal, frontal, parietal and occipital fit each other perfectly. The remaining
320 bones are matching in size, colour and texture. The skull is short and relatively wide (Length
321 from condyles to nasals = 540 mm, Width at the frontals \approx 190 mm), belonging to a large-
322 sized adult rhinocerotid. The separated nasal bones are long and longer than the preserved part
323 of the premaxilla, relatively thin and bear a lateral apophysis. Roughness for a small nasal
324 horn is preserved at the tip of the nasals. In lateral view, the foramen infraorbitalis and the
325 posterior border of the U-shaped nasal notch are both located above the P3, while the anterior
326 border of the orbit is above the M1. The minimum distance between the posterior edge of the
327 nasal notch and the anterior border of the orbit is 67.2 mm.

328 **Cranial features.** The skull was partly destroyed and some elements were reconstructed
329 in anatomical position by one of us (AS). It is short, broad, and elevated. The dorsal profile of
330 the skull is concave, with a small protuberance for a short nasal horn and an upraised parietal
331 bone (50°). In lateral view, the nasals have a small ventrolateral prominence (lateral
332 apophysis, sensu Antoine, 2002). The maxilla is badly damaged and the area of the foramen
333 infraorbitalis is restored on both sides. Nevertheless, based on the preserved part of the
334 maxilla, a position above P4 can be hypothesised. The posterior end of the nasal notch is
335 located above the anterior part of P3. The nasal septum is not ossified at all. The premaxillae
336 are broken rostrally. They form a short and elevated strip, slightly dipping forward, with a
337 deep ventral sulcus. Relations between nasal and lacrimal bones are not observable, and
338 neither are the lacrimal processi. The anterior border of the orbit is situated above the middle
339 of M1. On the frontal, a pair of smooth tubercles lay on the dorsal and posterodorsal edges of

340 the orbit (processus postorbitalis). The anterior base of the processus zygomaticus maxillari is
341 low, ~1 cm above the neckline of molars. The zygomatic arch forms a straight, low, and
342 oblique strip, with parallel dorsal and ventral borders. It is parallel to the dorsal outline of the
343 skull, with a rounded and rugose posterodorsal tip. A marked processus postorbitalis deforms
344 the dorsal edge of the zygomatic process, at the junction between the jugal and the squamosal.
345 Its tip, located on the latter bone, has a rugose aspect. Most of the temporal fossa elements are
346 not preserved and it is therefore impossible to consider the shape and relations of the foramina
347 sphenorbitale and rotundum. The area between the temporal and nuchal crests is depressed,
348 forming a deep gutter. The external auditory pseudo-meatus is partly closed ventrally. The
349 posterior side of the processus zygomaticus is flat in lateral view (no posterior groove). The
350 occipital side is inclined up- and forward, with a very salient nuchal tubercle (although small,
351 i.e., not extended on a wide area), determining a diamond-shape to the skull in dorsal view.
352 The occipital condyles are oriented in the same axis as the skull in lateral view. The posterior
353 tip of the tooth row reaches the posterior third of the skull. The pterygoids are not preserved,
354 as most of the basicranium, vomer, and basal foramina. The skull is brachycephalic
355 (interzygomatic width/total length ~0.57; Table 1). As observable in dorsal view, the nasals
356 have a sharp tip. They are long and unfused, fully separate by a deep groove from tip to tip.
357 There were no lateral nasal horns, but a small median nasal horn, as unambiguously shown by
358 the presence of axial vascularised rugosities in the anterior quarter of the nasal bones. In
359 contrast, the frontal bones have a smooth aspect, thus indicating the absence of a frontal horn.
360 The orbits were not projected laterally. The zygomatic arches are 1.51 times wider than the
361 frontals. From this frontal ambitus, run posteriorly two straight and smooth frontal crests,
362 getting closer by the parietals (minimum distance = 30 mm; Table 1), and then abruptly
363 diverging and forming an occipital crest that is concave posteriorly. The transition from the
364 maxilla to the processus zygomaticus maxillary is progressive, with no brutal inflection. The

365 articular tubercle of the squamosal is smooth (in lateral view) and straight (in sagittal view).
366 The right processus postglenoidalis forms a rounded right dihedron in ventral view. The
367 foramen postglenoideum is remote from the latter. The left one is not preserved. The occipital
368 side is wide and, accordingly, the processus posttympanicus and the processus paraoccipitalis
369 are distant. The former is poorly developed, while the latter is very long, slender, and vertical.
370 The foramen magnum is not preserved well enough to allow any observation. The occipital
371 condyle has a median ridge but no medial truncation.

372 **Mandible**

373 In lateral view, the symphysis is upraised, with an angular ventral profile determined by
374 two successive inflections. The foramen mentale is widely open and located below p2 (left)
375 and p3 (right). The corpus mandibulae is low, with a straight ventral border (Table 2). It is
376 getting gradually higher to the mandibular angle, smooth, rounded and hugely developed.
377 There is a shallow vascular incisure. The ramus is low, with a posterior border that is oblique
378 up- and forward and a vertical anterior border. The processus coronoideus is high, tapering
379 dorsally, and somewhat concave posteriorly. The condyloid process is high and sharp-edged,
380 separate from the latter by a deep mandibular notch. In dorsal view, the symphysis is massive,
381 well developed anteroposteriorly and narrow, with i2s and lateral edges parallel and two
382 circular alveoli for small i1s. The posterior border of the symphysis is located between the
383 trigonids of p3. The tooth rows are more parallel than the bodies (Fig. 4), which widely
384 diverge posteriorly. The spatium retromolare is wide on both sides. The mylohyoid sulci are
385 present but very shallow. The foramen mandibulare opens below the teeth-neck line.

386 **Dental material**

387 The dental formula is 1-0-4-3/2-0-3-3. No decidual dentition is known.

388 **Upper dentition** (Fig. 4, Table 3). The first upper incisors are not preserved, but
389 straight and sagittally-elongated alveoli point to an oval cross section for them (as usual in

390 teleoceratines). There are no I2, I3, or C. The premolar series is short with respect to the
391 molar series ($LP3-4/LM1-3 \times 100 = 48.7$; $Lp3-4/Lm1-3 \times 100 = 45.8$), which is further highlighted
392 by the small size of P2 and p2. The enamel is thick, wrinkled and corrugated, and partly
393 covered with a thin layer of cement. Teeth are low crowned, with roots partly joined. The
394 labial cingulum is absent on the upper cheek teeth. A thick paracone fold is present on P2-M3,
395 vanishing with wear on P2-M1 and marked until the neck on M2-3. There is no metacone fold
396 or mesostyle on the upper cheek teeth. Short and wide crochet is present on P3-4 (always
397 simple), but absent on P2. There is no metaloph constriction on P2-4. The lingual cingulum is
398 absent on all upper cheek teeth, except for a small tubercle on the anterolingual base of the
399 hypocone on both P4. The postfossette forms a small and deep isometric pit. The antecrochet
400 is getting stronger backward, from absent on P2 and short on P3-4 to very elongate on M1-3.
401 The first upper cheek tooth is most likely a persistent D1: it is much more worn than other
402 teeth and the enamel is also much thinner. It is preserved on the right side and its presence is
403 further attested by two alveoli on the left side (heart-shaped anterior root; peanut-shaped
404 posterior root). It has a sharp anterolingual cingulum, a straight lingual edge, and rounded
405 posterior and labial edges. P2-4 are fully molariform (bilophodont, with an open lingual
406 valley). On P2, the metaloph is transverse labially, but curved posterolingually due to the
407 position of the hypocone. The latter is much more developed than the protocone. The
408 protoloph is thin but continuous and transversely oriented. There is no medifossette on P3-4,
409 but a short crista on P4 and on P3 (mostly wiped out by wear on P3). The protocone is
410 constricted anteriorly on P3-4. The metaloph forms a dihedron on P3-P4, with the crochet as a
411 tip and the hypocone located posterior to the metacone. The protoloph is complete and
412 continuous and there is no pseudometaloph on P3. The metacone is not constricted or isolated
413 on P3-4. The crochet is long and sagittal on M1-M3, with a rounded tip on M1, and a sharp
414 tip on M2-3. There is no crista, medifossette, or cristella on upper molars. The lingual

415 cingulum is restricted to a small pair of tubercles on M2s and a smooth ridge on the hypocone
416 of M3. The protocone is strongly constricted on M1-3, and trefoil shaped on M3. The
417 parastyle is short and sagittal on M1-3; the paracone fold is very salient on M2 and especially
418 on M3. The metastyle is very long on M1-2. The metaloph is almost as long as the protoloph
419 on M1-2. In lingual view, the protocone is increasingly developed sagittally from M1 to M3.
420 A deep groove carves the anterolingual side of the hypocone on M2, and a shallower one is
421 observed on M1. The ectoloph is straight on M1 and concave on M2. The antecrochet and the
422 hypocone are close but separate on M1-2. There is no lingual groove on the lingual side of
423 M2. The posterior cingulum is complete on M1-2 and the postfossette is still narrower and
424 deeper than on premolars. The right M3 has a triangular outline in occlusal view, with a
425 straight ectometaloph (the left M3 is not preserved). The protoloph is transversely developed.
426 There is no posterior groove on the ectometaloph and the labial cingulum is restricted to a low
427 and smooth spur covering the lingual third of the former.

428 **Lower dentition** (Fig. 4, Table 3). There are small circular alveoli for both i1s, between
429 the i2s, in the symphyseal part of the dentary but the shape of the concerned teeth is unknown.
430 The presence of a short p2 is attested by three closely-appressed alveoli on the right side (area
431 unpreserved on the left side), but no d1 or p1 was present, as attested by the sharp ridge
432 running anterior to p2's alveoli. There are no vertical rugosities on the ectolophid of p3. On
433 the lower cheek teeth, ectolophid grooves are developed (U-shaped) and vanishing before the
434 neck, trigonids are rounded and forming a right angle in occlusal view, metaconids and
435 entoconids are unconstricted. The bottom of the lingual valleys is V-shaped in lingual view on
436 lower premolars. On lower premolars, the lingual cingulum is restricted to a low ridge
437 continuing the anterior cingulum on the trigonid of p3s, and the labial cingulum consists of a
438 small edge obtruding the ectolophid groove on p4s. Lower molars lack a lingual cingulum but
439 a small cingular ridge partly obtrudes the ectolophid groove. The hypolophid is oblique in

440 occlusal view on m1-3. There is no lingual groove on the entoconid of m2-3. The posterior
441 cingulum of m3 forms a low, horizontal, and transversely-elongated ridge.

442 **Poscranial skeleton** (Tables 4, 5)

443 **Atlas.** The atlas is wide and short sagittally. In dorsal view, the transverse processes
444 (partly broken) and the alar notches are developed and the axis-facets are concave. In anterior
445 view, the rachidian canal has a bulb-like outline. The occipital condylar facets are kidney-like.
446 The foramen vertebrales cuts across the anterior third of the dorsal surface on both sides and it
447 is continued by a shallow groove laterally (for the vertebral artery). In posterior view, the
448 foramen transversarium is present, wide and partly hidden by the lateral expansion of each
449 axis-facet (Fig. 5, A).

450 **Axis.** The axis is stocky, with thick and cylindrical dens and tear-shaped atlas-facets
451 (convex transversely) on the prezygapophyses. The spinous process is thick and carinated.
452 The foramen vertebrales is large and subtriangular. The postzygapophyses have wide and
453 circular facets for the first thoracic vertebra, forming a $\sim 45^\circ$ angle with the horizontal line.
454 The centrum is very long anteroposteriorly, with a pentagonal outline in posterior view (Fig.
455 5, B). Most thoracic vertebrae are preserved. They are massive, with heart-shaped centroms,
456 and stocky transverse processes. The dorsal spines are slender and oblique (45° with the
457 vertical line), with a length reaching up to 250% of the centrum height for the T4-6.

458 **Scapula.** The scapulae are partly preserved. They are elongated dorsoventrally, notably
459 due to their anteroposterior narrowness ($H/APD = \sim 0.50$). The scapular spine is straight,
460 much developed and with an extremely salient tuberculum bent caudally. There is no pseudo-
461 acromion. The tuberculum supraglenoidale is well distinct from the cavitas glenoidalis. The
462 medial border of the cavitas glenoidalis is straight, determining a semi-circular outline in
463 ventral view.

464 **Humerus.** Both humeri are almost complete (Fig. 6, A-E). The humerus is a slender
465 bone, with a straight diaphysis. The trochiter is high, with a smooth and rounded outline. The
466 caput humeri is wide and rounded, with a rotation axis forming a 40° angle with the vertical
467 line. The deltoid crest is elongated, almost reaching the mid-bone. The deltoid tuberosity is
468 not much salient. The fossa radii is wide and shallow. The fossa olecrani is higher than wide.
469 The distal articulation is egg-cup shaped (sensu Antoine, 2002, 2003), without marked median
470 constriction. The trochlea is half-conical and the capitulum humeri is half-cylindrical. There is
471 no synovial fossa (“trochlear scar”) on the anterodorsal edge of the trochlea. The lateral
472 epicondyle is elongated dorsoventrally and its ventral border ends dorsal to the capitulum
473 humeri, lacking a distal gutter.

474 **Radius.** The two bones are complete and undistorted (Fig. 06, F-J). The anterior border
475 of the proximal articulation is straight in dorsal view but convex in anterior view. The radius
476 is slender, with a distal extremity larger than the proximal one in anterior view. The diaphysis
477 is quite slender, especially in its proximal half. It has a straight medial border in anterior view,
478 but it is posterolaterally concave, which determines a wide spatium interosseum brachii when
479 the ulna is in anatomical connection. The proximal ulnar facets are fused on both sides. The
480 insertion of the m. biceps brachii is wide but shallow, with two small pits. Ulna and radius are
481 independent, apart from the proximal and distal articular areas. On the anterodistal part of the
482 diaphysis, the gutter for the m. extensor carpi is not marked at all. There is only one distal
483 facet for the ulna on the lateral side of the bone. The posterior expansion of the scaphoid-facet
484 is high, forming a right-angled rectangle. There is a wide pyramidal-facet on the distal
485 articulation.

486 **Ulna.** The bone is sturdy, with a long and heavy olecranon, the tip of which is wide and
487 diamond shaped (Fig. 6, K-O). The diaphysis is straight, triangular in cross- section and as
488 robust as the radius shaft. It forms a ~135° angle with the olecranon in lateral view. The

489 humeral facet is saddle-shaped. The proximal radio-ulna facets form a continuous pad, with a
490 wide medial strip and a high triangular lateral facet. A smooth but salient anterior tubercle is
491 located above the distal end of the bone. There is neither a second distal radius-facet on the
492 medial side of the diaphysis nor semilunate-facet on the distal side. The almond-shaped distal
493 radius-facet is separate proximally from a salient horizontal ridge by a deep and rugose
494 depression. The pyramidal-facet is concavo-convex, with a quarter-circle outline in distal
495 view.

496 **CARPUS.** The carpus is very low and massive, especially with respect to slender
497 stylopodial and zeugopodial elements (Fig. 7). All carpals have salient tubercles on the
498 anterior aspect of the bones. The right hand is more complete than the left one.

499 **Scaphoid.** The scaphoid is low and massive, with equal anterior and posterior heights
500 (Fig. 7, A-C). The proximal radial facet is diamond shaped in proximal view. The
501 posteroproximal semilunate facet is strongly distinct. It is oval, wide, and separated from all
502 other facets. A deep depression hollows the lateral side between the semilunate-facets. The
503 anterodistal semilunate-facet is nearly flat and crescent shaped. The magnum-facet is concave
504 in lateral view. The trapezium-facet is smaller than other distal facets, but it forms a wide
505 triangle, separated from the trapezoid-facet by a smooth ridge.

506 **Semilunate.** The bone is compact. In proximal view, the anterior facet only contacts the
507 radius, whereas the wide posteromedial facet is for the scaphoid (Fig. 7, F-I). The anterior
508 side is smooth (not keeled or carinated), with a sharp distal tip. On the lateral side, both
509 pyramidal-facets are closely appressed. The proximal one is almond shaped and the distal one
510 is comma like. The posterior tuberosity is short. Most of the distal side is articulated, medially
511 with the magnum and laterally with the unciform.

512 **Pyramidal.** The bone is almost cubic. The proximal side is square shaped, with a
513 saddle-shaped ulna-facet (Fig. 7, J-M). The semilunate-facets are sagittally elongated, with a

514 half-oval outline for the proximal one and a crescent-like shape for the distal one. The
515 pisiform-facet is comma shaped, with a concave sagittal profile and it overhangs a strong
516 lateral tuberosity. The distal facet, for the unciform, forms a right isosceles triangle with
517 rounded angles. There is no magnum-facet.

518 **Pisiform.** The right pisiform is short, high, and spatulate, with large and triangular
519 radius- and pyramidal-facets (Fig. 7, N-P). Both facets are separated by a sharp ridge and
520 form a right angle. There is no strong constriction separating the thick body and the
521 articulated part. The medial edge of the body is straight and vertical.

522 **Trapezium.** The right trapezium is preserved. It is a small proximo-distally flattened
523 bone with a circular outline in proximal view. The proximal side is almost entirely occupied
524 by a wide pentagonal scaphoid-facet (compatible with the large-sized trapezium-facet on the
525 scaphoids). The latero-distal side bears a trapezoid-facet with a right-triangled shape,
526 overhanging a deep pit. All other sides have a rugose aspect and they are devoid of articular
527 facets.

528 **Trapezoid.** Only the right trapezoid is documented (Fig. 7, D-E). It is wider than high,
529 almost cubic. Only the anterior and posterior sides (oval and pentagonal in shape,
530 respectively) are free of articular surfaces. The proximal side, saddle shaped and tapering
531 posteriorly, responds to the scaphoid. In medial view, the trapezium-facet is restricted to the
532 posterior half, with a deep insertion pit located close to the anterior edge. The lateral facet is
533 a low rectangle for the magnum. The distal side is weakly concavo-convex, and it consists of
534 a pentagonal McII-facet.

535 **Magnum.** The magnum has a very low anterior aspect, with a subrectangular outline
536 and a salient horizontally-elongated median pad (Fig. 7, Q-T). The proximal border is straight
537 in anterior view. In medial view, the anteromedial facets are in contact throughout their whole
538 length (no anterior groove). In lateral view, the dorsal pulley for the semilunate forms a low-

539 diameter half circle, further determining a question mark proximal profile. The distal facet is
540 wide and tapering posteriorly. The posterior tuberosity is broken on the left magnum, and it is
541 very short on the right specimen.

542 **Unciform.** The bone is compact, with a posterior tuberosity wide and much developed
543 sagittally (Fig. 7, Y-W). The anterior side is wide and low, with a pentagonal outline and a
544 maximum height on its lateral tip. The proximal side has two anterior facets flat transversally
545 and convex sagittally, separated by a sharp sagittal edge. The medial one, triangular, is for the
546 semilunate while the lateral one, diamond shaped, is for the pyramidal. The latter has a wide
547 posterolateral expansion joining the lateral edge and the McV-facet (located on the distal side)
548 on the right unciform. This part is broken on the left one. From the medial tip, the distal and
549 distolateral sides have three contiguous facets, responding to the McIII (small and
550 quadrangular), McIV (bulb-shaped), and McV (oval and deeply concave sagittally),
551 respectively. They are only separated by smooth sagittal grooves. The McV-facet is oblique,
552 which could suggest the presence of a functional McV (see Antoine, 2002, 2003; Boada-Saña
553 et al., 2008).

554 **METACARPUS.** The hand and pes have a mesaxonian Bauplan. Although no McV is
555 preserved, the hand was probably tetradactyl, as hypothesised by the vertical facet on the
556 McIV (see above). The metapodials have salient insertions for the m. extensor carpalis. Their
557 shafts are robust (wide transversally and flattened sagittally), with neither distal widening nor
558 clear shortening (no brachypody; see Antoine, 2002). The insertions for the m. interossei are
559 long, reaching the mid-shaft on all available metapodials. The intermediate reliefs do not
560 reach the anterior aspect of the distal articulation on metapodials. The intermediate relief is
561 moderately high and quite sharp on the McIII, but low and smooth on medial and lateral
562 metapodials.

563 **McII.** In proximal view, the proximal side consists of a large tear-shaped trapezoid-
564 facet medial to a narrow sagittally-elongated and strip-like magnum-facet. In medial view, the
565 trapezium-facet is large and comma shaped, higher in its posterior tip. In lateral view, the
566 magnum-facet is a straight and low strip, separated from the McIII-facets over their length.
567 The McIII-facets are fused into a curved strip with a shallow disto-median constriction. The
568 distal articulation, for the phalanx 1, has a sub-square outline in distal view, with rounded
569 anterior angles. Above it, is a wide and salient medial tuberosity (Fig. 8, A-E).

570 **McIII.** The bone has a straight shaft. The proximal side is dominated by a wide and
571 pentagonal magnum-facet, contiguous to two narrow sagittal strip-shaped facets (medially for
572 the McII and laterally for the McIV). In anterior view, the proximal side consists of a
573 subvertical medial edge (McII-facet), a very wide magnum-facet, weakly-concave medially,
574 and a much narrower, oblique and straight McIV-facet. The magnum-facet is almost invisible
575 in anterior view. Indeed, its dorsal outline is not much convex in medial view. The McII-
576 facets are broadly connected, forming a thick strip with a shallow constriction in its disto-
577 median part. In lateral view, the anterior McIV-facet is low, elongated sagittally, and tear-
578 shaped. It is disconnected from the oval posterior McIV-facet by a narrow but deep oblique
579 groove. This articulated surface overhangs a deep circular depression. There is no postero-
580 distal tubercle on the diaphysis. In distal view, the distal articulation is wide and
581 subrectangular, with straight medial and lateral edges, rounded antero-medial and -lateral
582 angles, and a m-like posterior edge, due to a low but sharp intermediate relief (Fig. 8, F-J).

583 **McIV.** The McIV is the shortest and most robust metapodial preserved. The shaft is
584 concave laterally in anterior view. The proximal aspect is trapezoid, deeper than wide, with a
585 narrow medial strip (the sagittally-elongated ‘anterior’ McIII-facet) and a wide unciform-
586 facet. In proximal view, there is no postero-lateral pad, but a small anterolateral tubercle in
587 front of the McV-facet. In medial view, the proximal McIII-facets are connected (right

588 specimen) and form a right dihedron (L-shape), with a high posterior facet. The McV-facet is
589 vertical, suggesting a functional McV, in good agreement with the orientation of the McV-
590 facet on the unciform. In distal view, the distal articulation forms a quarter circle, with a
591 posteromedial right angle. There is almost no intermediate relief on the McIV (Fig. 8, K-O).

592 **Phalanges.** Only three phalanges are preserved for the manus (left/right first phalanges
593 and left second phalanx for the McII). They have strong interphalangeal insertions and
594 tubercles. The phalanx 1 is low and massive, with a kidney-like proximal side (McII-facet,
595 lacking a groove responding to the intermediate relief). The distal facet is oval and
596 transversely transversally elongated. The phalanx 2 is still lower, with a proximal facet
597 perfectly matching in shape the distal facet on the phalanx 1. The distal facet is slightly
598 concave transversally and convex sagittally. Both facets have similar width and depth.

599 **Coxal.** The pubic bones and ischia are lacking on both sides but the ilia are well
600 preserved. Dorsally, the iliac crest is regularly convex. The wing of the ilium is spatulated.
601 The sacral tuberosity has a rounded triangular shape, with a rugose aspect. The coxal
602 tuberosity, partly broken, was probably thick and high, also with a rugose aspect. The caudal
603 gluteal line is smooth, with a concave outline (forming a semi-circular curve). The
604 acetabulum has a subcircular outline.

605 **Femur.** The bone is quite slender, with a shaft straight in anterior view, concave
606 anteriorly in lateral view, and compressed sagittally (Fig. 9, A-F). The anterior part of the
607 trochanter major is high, but the caudal part is very low, i.e., much lower than the wide and
608 hemispheric head. The fovea capitis is deep, low, and wide, with a triangular outline. The
609 trochanter minor is elongated dorsoventrally. Its distal end reaches the mid-height of the third
610 trochanter. The latter is developed, wider distally and with smooth lateral borders. The
611 anteroproximal border of the patellar condyle is curved, with a medial lip much more
612 developed and salient than its lateral counterpart. In lateral view, the medial lip of the trochlea

613 and the diaphysis determine a broken angle (130°). In distal view, the anterior border of the
614 patellar trochlea is convex medially and straight and transverse laterally. The tibial condyles
615 are separate from the patellar trochlea by a narrow groove. The intercondylar fossa is deep
616 and narrow. The medial condyle, with a diamond-shaped outline, is much more developed
617 than the lateral one. The medial epicondyle is also more salient than the lateral epicondyle.

618 **Patella.** The patella is massive, wider than high, and with a triangular and rugose
619 anterior aspect. The medial border is straight and vertical. The posterior side, almost fully
620 articulated, contacts the femoral cochlea, with a wide medial lip, triangular (wider distally),
621 and a narrower trapezoid lateral lip. In vertical view, the latter lip is almost straight while the
622 former is more concave. The most striking feature is the weak anteroposterior development of
623 the bone with respect to other dimensions.

624 **Tibia.** The tibia is high and relatively slender, with heavy extremities (Fig. 9, K-O). The
625 medial border of the diaphysis is strikingly straight in anterior view, which widely contrasts
626 with the concave lateral border of the shaft. This impression is highlighted by the median half
627 of the proximal articulation being much higher than the lateral one. The patellar ridge is thick
628 and bulbous, with a rough surface. The patellar groove is deep, short dorso-ventrally, and
629 regularly concave. The proximal peroneal articulation is located low on the tibia (no contact
630 with the lateral femoral condyle). There is neither an anterodistal groove nor medio-distal
631 gutter (for the tendon m. tibialis posterior). Tibiae and fibulae are independent, apart from
632 articulated areas, thus determining a wide spatium interosseum cruris. The distal fibula-facet
633 is low, elongated, and crescent shaped, overhung by a rugose triangular area. The posterior
634 apophysis is low and rounded. In distal view, the outline is a trapezoid, wider than deep. The
635 astragalar cochlea has two lips, the medial one being narrower and deeper and the lateral one
636 wider and shallower.

637 **Fibula.** The diaphysis is straight and particularly slender, in sharp contrast with two
638 thick ends (and the robustness of the tibia) (Fig. 9, G-J). The proximal end is nevertheless
639 flattened sagittally, with a smooth proximal tibia-facet. The distal end is robust, with a deep
640 laterodistal gutter for the tendon m. peroneus, located posteriorly, immediately posterior to a
641 huge tubercle. The distal fibula-facet is low, elongated sagittally, and crescent shaped. It is
642 contiguous to a flat and rectangular astragalus-facet, oriented at $\sim 25^\circ$ with respect to the
643 vertical line.

644 **PES.** The pes is not completely known (Fig. 10). The naviculars, cuneiforms, MtIII, and
645 most phalanges are not preserved. The metatarsals are shorter than the metacarpals.

646 **Astragalus.** The astragalus is thick ($APD/H = 0.76$), wide and low ($TD/H = 1.29$). The
647 fibula-facet is subvertical, wide and flat dorsoventrally (Fig. 10, A-C). The medial trochlear
648 ridge is rounded, whereas the lateral one is sharper. The collum tali is very high (up to $\frac{1}{4}$ of
649 the height), especially with respect to the general proportion of the bone. The caudal border of
650 the trochlea is sinuous in dorsal view (with a falciform shape). There is no anterodistal
651 trochlear notch, but a wide foramen for an insertion located distally to the concerned area, in
652 the mid-collum tali. In anterior view, the distal border is deeply concave medially (navicular-
653 facet) and straight and oblique laterally (cuboid-facet). The medial tubercle is low and
654 rounded, but much projected medially. The distal articulation is not twisted with respect to the
655 axis of the trochlea ($< 15^\circ$), in distal view. The calcaneus-facet 1 has a wide and very low,
656 triangular laterodistal expansion. This facet is nearly flat in lateral view. The calcaneus-facets
657 2 (low oval) and 3 (tear shaped and low) are distinct and separate by a wide groove. In distal
658 view, the distal articulation is much wider than deep, with a cuboid-facet particularly wide
659 transversely. The posterior stop on that cuboid-facet is abrupt and prolonged medially by a
660 similar transversely-elongated inflection on the navicular-facet.

661 **Calcaneus.** The calcaneus is robust, with a tuber calcanei massive and oval in
662 posteroproximal view (Fig. 10, D-F). This tuber calcanei is strongly vascularised and rugged
663 with salient muscle/tendon insertion areas, The tibia-facet is low, wide, and almond shaped,
664 while the fibula-facet is round and oblique with respect to the vertical and sagittal lines. The
665 astragalus-facet 1 is lozenge shaped in anterior view and almost flat. The facet 2 is oval, wider
666 than high and flat. It is separate from the smaller and semi-oval facet 3. The sustentaculum
667 tali is low and very wide. In lateral view, the cuboid-facet and the posterior border of the tuber
668 form a right angle and the processus, at the level of the sustentaculum tali, is deeper (in terms
669 of APD) than the tuber calcanei. The insertion for the m. fibularis longus forms a salient and
670 rugose pad, but without sharp ridges. On the distal side, the cuboid-facet forms a transversely-
671 elongated hexagon. It is mostly flat but concave in its mediolateral quarter.

672 **Cuboid.** The cuboid is compact, wide, and low (Fig. 10, G-I). In proximal view, the
673 large articular surface is oval, slightly tapering posteriorly, and split into two equally-
674 developed and sagittally-elongated facets. The astragalus-facet (medial) is separated from the
675 calcaneus-facet (lateral) by a narrow and shallow groove. The anterior side is low and
676 pentagonal in anterior view, with a sharp proximal tip. In medial view, there are four facets.
677 The anteroproximal one is very low and crescent like (navicular-facet). Distally to it is a much
678 larger semi-circular ectocuneiform-facet. The posteroproximal navicular-facet, broadly
679 joining the proximal facet for the astragalus, has an 8-shaped outline. Contiguous to it, but
680 distally, is a semi-circular posterodistal ectocuneiform-facet. The posterior tuberosity is short
681 sagittally and narrow, but quite elevated: its acuminated distal tip is positioned much more
682 distally than the distal articulation (MtIV-facet). The latter facet is flat and trapezoid, with
683 larger anterior, medial, and posterior sides and a shorter lateral border. There is no MtIII-
684 facet.

685 **MtIII.** The bone is short and robust (Fig. 11, A-E). The proximal side, with a triangular
686 outline (widening posteriorly), responds to the entocuneiform (posteromedial facet,
687 pentagonal, and oblique), the mesocuneiform (proximal-most facet, wide and trapezoid), and
688 to the ectocuneiform (wide strip-like facet oblique and tapering anteriorly). In lateral view, the
689 MtIII-facets are vertical, with a large triangular anterior facet and a much lower, oval
690 posterior facet. Both are widely connected. The shaft is straight and subcircular in cross
691 section. The distal end is stocky and square in distal view. The distal articulation has almost
692 no intermediate relief, even in its posterior aspect.

693 **MtIV.** The bone is short and massive, with a heavy proximal end (Fig. 11, F-J). The
694 proximal side is entirely occupied by a flat and sub-square cuboid-facet. There are two
695 distinct proximal tubercles at the anterolateral and posterolateral angles, but no continuous
696 pad. In medial view, there are two equally-wide MtIII-facets. The anterior one is located more
697 dorsally, elevated and with a half-oval outline, connecting the proximal side. The posterior
698 one is oval, isolated, and anteroventrally-posterodorsally elongated. The shaft is slightly
699 concave laterally but straight in lateral view, with a strong laterodistal tubercle. The distal side
700 is entirely articulated, deeper than wide (APD>TD), and lacking an intermediate relief. Only
701 the lateral lip is slightly concave transversely in its posterior aspect.

702 **Phalanges.** Only the first phalanges for the MtII and MtIV are known. They have strong
703 interphalangeal insertions and tubercles. There is no groove responding to the intermediate
704 relief. The MtII phalanx 1 is almost cubic, with a circular and slightly biconcave proximal
705 side (MtII-facet). The distal facet (phalanx 2) is kidney shaped. The MtIV phalanx 1 is as
706 wide as but lower than the former phalanx. The proximal facet is kidney shaped and almost
707 flat. The distal facet is oval and elongated transversely. In both phalanges, the distal facet is
708 smaller than the proximal facet, but also slightly convex sagittally and concave transversely.

709 COMPARISON

710 In the next paragraphs, the comparison will be organised following anatomical regions (skull,
711 mandible, teeth, and postcranial skeleton) and we will use the generic assignments as
712 supported by the phylogenetic analysis.

713 The rhino from Tagay cannot be assigned to *Diaceratherium* (*sensu stricto*, see below) as it
714 does not have teeth with wrinkled enamel, M1-2 with a short metaloph, M2 with a mesostyle,
715 semilunates with a distal border of the anterior side rounded, or unciforms with a posterior
716 expansion of the pyramidal-facet always present (all these features are diagnosing its type and
717 only species, *D. tomerdingense*). It cannot belong either to *Brachypotherium*, the
718 representatives of which have an occipital condyle without a median ridge, a mandibular
719 symphysis very massive, a labial cingulum usually present on upper premolars and always
720 present on upper molars, lower cheek teeth with a flat ectolophid, lower premolars with a
721 lingual opening of the posterior valley U-shaped, p2 with a paraconid reduced, radius-ulnae
722 with a second distal articulation, pyramidals with a distal semilunate-facet asymmetric,
723 posterior facet always absent on the McII-McIII, and a fibula-facet oblique on the astragali.
724 Contrary to representatives of *Prosantorhinus*, it has no sagittal fronto-parietal crest, posterior
725 groove on the processus zygomaticus of the squamosal, or metacone fold on M1-2, but a
726 constricted metaloph on M1 (diagnostic features of the genus). At last, it is differing from
727 *Teleoceras fossiger* in a wide array of cranio-mandibular, dental, and postcranial features
728 (e.g., foramen infraorbitalis above premolars, processus postorbitalis present on the zygomatic
729 arch, occipital side inclined up-and frontward, low-crowned cheek teeth, crista always present
730 on P3, atlas with a bulb-like rachidian canal cavity, scapula elongated, or navicular with a
731 lozengic outline in vertical view).

732 On the other hand, in its general shape, proportions and anatomical features, the skull from
733 Tagay closely matches that of *Brachydiceratherium shanwangense* (Wang, 1965) as recently
734 described by Lu et al. (2021). It also resembles that of late Oligocene–early Miocene

735 teleoceratines from Western Europe classically assigned to *Diaceratherium*, except for the
736 type species (*D. tomerdingense*, for which only an isolated nasal bone is preserved). Within
737 *Brachydiceratherium*, the arched dorsal profile, the short and slender premaxillae, the
738 zygomatic arch (straight, oblique, with a marked posterodorsal angle, and an anterior tip
739 starting progressively), and the processus paraoccipitalis long and narrow make it have the
740 closest affinities with *Bd. shanwangense*, *Bd. aginense* (earliest Miocene; Répelin, 1917), and
741 *Bd. asphaltense* (Becker et al., 2018). The only differences with the former do concern the tip
742 of the nasal bones, pointing upward, having a small median bump (suggesting the presence of
743 a terminal nasal horn) and a distolateral apophysis, and the stockier zygomatic arch as
744 observed in the Tagay specimen. More specifically, the Tagay skull differs from that of *Bd.*
745 *aginense* in having a processus postorbitalis on the frontal bone and a median ridge on the
746 occipital condyle, but no posterior groove on the processus zygomaticus of the squamosal
747 (Répelin, 1917). It is distinct from *Bd. lemanense* in possessing a low zygomatic arch, with a
748 processus postorbitalis, a small processus posttympanicus and a well-developed processus
749 paraoccipitalis (Lavocat, 1951), and from *Bd. asphaltense* in having closer fronto-parietal
750 crests and a brachycephalic shape (Becker et al., 2018; Jame et al., 2019). In contrast, the
751 shape of the processus zygomaticus, but also the presence of a small median nasal horn and of
752 a concave occipital crest make it somewhat resemble *Bd. asphaltense*.

753 As for mandibular features, the Tagay jaw is also particularly resembling those of *Bd.*
754 *shanwangense* and *Bd. aginense* among representatives of *Diaceratherium*, with an upraised
755 symphysis (distinct from that of *Bd. lamilloquense* and of *Bd. aurelianense*), low corpus,
756 vertical ramus and a deep and laterally-salient mandibular angle, with a shallow vascular
757 incisure.

758 With respect to all other representatives of *Diaceratherium* now referable to
759 *Brachydiceratherium* (see phylogenetic discussion), the most distinctive dental features of the

760 Tagay rhinocerotid are a short premolar series (also observed in *Bd. shanwangense*), an
761 enamel wrinkled and corrugated at the same time, crochets simple and lingual cingula usually
762 absent and always reduced on P2-4, a protocone strongly constricted on M1, a lingual
763 cingulum usually absent on lower premolars and always absent on lower molars, and the
764 absence of d1/p1 at an adult stage (also observed in *Bd. shanwangense*). It can be further
765 distinguished from *Bd. lamilloquense*, *Bd. lemanense*, *Bd. asphaltense*, and/or *Bd.*
766 *aurelianense* by its I1s oval in occlusal view, the absence of labial cingulum on upper
767 premolars and molars, the presence of a strong paracone fold on M1-2 and of a constricted
768 hypocone on M1, and M3s with a triangular occlusal outline. Contrary to *Bd. lamilloquense*,
769 the rhino from Tagay has a protoloph joined to the ectoloph on P2, but also a protocone and a
770 hypocone lingually separate on P3-4 (molariform). With respect to *Bd. aurelianense*, it has no
771 metaloph constriction on P2-4 and a protocone weakly developed on P2. In other words,
772 dental remains from Tagay are strictly similar to those of *Bd. shanwangense* (Lu et al., 2021).
773 They further have very close affinities with those of *Bd. aginense* and *Bd. intermedium* among
774 *Brachydiceratherium* representatives. Nevertheless, the Tagay rhinocerotid differs from *Bd.*
775 *aginense* in bearing a protocone and a hypocone lingually separate on P2 (molariform) and
776 from both species in having a long metaloph on M1-2 and a posterior groove on M3.
777 Even though postcranial elements are not known in all *Brachydiceratherium* species, the
778 cervical vertebrae and/or limb bones from Tagay are perfectly matching those of *Bd.*
779 *shanwangense* (Lu et al., 2021). They are also very similar to those of *Bd. aginense* and of *Bd.*
780 *intermedium*, notably in terms of size and proportions. They differ, however, from all
781 representatives of the genus (including the latter species), in having a scapular glenoid fossa
782 with a straight medial border and a tibia-facet on the calcaneus, but no distal gutter on the
783 humeral lateral epicondyle. It can be further distinguished from *Bd. lamilloquense*, *Bd.*
784 *lemanense*, *Bd. asphaltense*, and/or *Bd. aurelianense* by a radius with a high posterior

785 expansion of the scaphoid-facet, a femoral head hemispheric, an astragalus with a laterodistal
786 expansion, the presence of very low-and-smooth intermediate reliefs on metapodials but also
787 a long insertion of m. interossei on lateral metapodials. The Tagay rhinocerotid differs from
788 *Bd. aginense* in bearing a shallow gutter for the m. extensor carpi on the radius, a posterior
789 MtII-facet developed on the Mt3, but no contact between the cuboid and the MtIII, from *Bd.*
790 *intermedium* in showing a right angle between the cuboid-facet and the base of the tuber
791 calcanei on the calcaneus, and from both species in having a scaphoid with equal anterior and
792 posterior heights, a short posterior tuberosity on the magnum, a wider astragalus (TD/H>1.2),
793 and a fibula-facet on the calcaneus.

794 In fact, the Tagay rhinocerotid individual is identical in all aspects to corresponding
795 specimens of the complete skeleton from the early Miocene of eastern China recently
796 assigned to as *Diaceratherium shanwangense* by Lu et al. (2021). The only differences lie in
797 the occipital crest being more concave in the Tagay skull than in the Shanwang one, following
798 the description by Lu et al. (2021). This feature is likely to document either sexual
799 dimorphism, ontogenetic variation, or interindividual variability. Accordingly, we consider
800 unambiguously the Tagay rhinocerotid as documenting *Brachydiceratherium shanwangense*.

801 PHYLOGENETIC ANALYSIS

802 We have first run a preliminary analysis (see supplementary materials: files S1 and S2),
803 with 32 taxa i.e., the Tagay individual and *B. shanwangense* scored as two distinct terminals.
804 In that analysis, these terminals differ in a single and only feature (char. 36: occipital crest
805 concave in the former). Accordingly, we have merged them into a single terminal, for running
806 the final analysis (see supplementary materials: files S3 and S4). A single most parsimonious
807 tree is retrieved (length = 1316 steps; consistency index = 0.2698; retention index = 0.4918;
808 Fig. 13; see supplementary files S3 and S4). Twenty-four characters are constant, due to their

809 original definition for solving phylogenetic relationships within Elasmotheriina (Antoine,
810 2002), a rhinocerotid subtribe the representatives of which are not included here. Character
811 distribution at each node and corresponding indices are detailed in the supplementary
812 materials (file S4). Suprageneric relationships within Rhinocerotinae (i.e., the clade including
813 Rhinocerotini + Aceratheriini) are consistent with those proposed by Antoine (2002, 2003),
814 Antoine et al. (2010, 2022), Becker et al. (2013), Tissier et al. (2021), and Pandolfi et al.
815 (2021): *Plesiaceratherium mirallesi* is the earliest offshoot among Rhinocerotinae (node 1; 26
816 unambiguous synapomorphies; Bremer Support [BS] > 5). Aceratheriini (node 3; nine
817 unambiguous synapomorphies; BS = 2) and Rhinocerotini (node 5; eight unambiguous
818 synapomorphies; BS = 2) are sister clades (node 2; 13 unambiguous synapomorphies; BS =
819 4). Rhinocerotina (node 6; 18 unambiguous synapomorphies; BS > 5) and Teleoceratina
820 (node 13; five dental and postcranial unambiguous synapomorphies; BS = 1) are sister clades
821 within Rhinocerotini (Fig. 13). Aceratheriini comprise *Alicornops simorreense* as a sister
822 species to the (*Aceratherium incisivum*, *Acerorhinus zernowi*) clade (node 4). Rhinocerotina
823 include the (*Lartetotherium sansaniense*, *Gaindatherium browni*) clade (node 7; seven
824 unambiguous synapomorphies; BS = 5) as the first offshoot, then *Nesorhinus philippinensis*
825 (node 8; seven unambiguous synapomorphies; BS = 3), and the living rhino species (node 9;
826 nine unambiguous synapomorphies; BS = 2), with the *Rhinoceros* clade (node 10; four
827 unambiguous synapomorphies; BS = 1) being sister group to the (*Dicerorhinus sumatrensis*
828 plus African rhinos) clade (node 11; 13 unambiguous synapomorphies; BS = 3). The clade of
829 living African rhinos is the most supported node of the tree (node 12; 38 unambiguous
830 synapomorphies; BS > 5).

831 In the next paragraphs, we will focus on the topology, node support (Bremer Support:
832 BS), and apomorphy distribution regarding the Teleoceratina. The monophyly of the subtribe
833 is weakly supported by five dental and postcranial unambiguous synapomorphies (BS = 1): 11

834 with an almond-shaped cross section, hypocone isolated by an anterior constriction on M2,
835 ulna with the olecranon and the diaphysis forming a closed angle, robust limbs, and lateral
836 metapodials with insertions of the m. interossei short. The earliest-diverging teleoceratine is
837 *Diaceratherium tomerdingense*. This species is defined by ten dental and postcranial
838 autapomorphies (teeth with enamel wrinkled and roots separate, P2-3 with an antecrochet
839 usually absent, M1-2 with a metaloph short, M2 with a mesostyle, humerus without a distal
840 gutter on the lateral epicondyle, semilunate with a distal border of the anterior side rounded,
841 trapezoid with a proximal border asymmetric in anterior view, unciform with a posterior
842 expansion of the pyramidal-facet always present, and trapezium-facet always absent on the
843 McII; Table 6). Next node (node 14) segregates the *Brachypotherium* clade (node 15) from all
844 other teleoceratines scored here (node 16). Node 14 (BS = 2) is weakly supported by three
845 postcranial unambiguous synapomorphies (proximal ulna-radius facets usually fused, gutter
846 for the m. extensor carpi weakly developed on the radius, and McII with anterior and posterior
847 McIII-facets fused). Eleven cranio-mandibular, dental, and postcranial synapomorphies define
848 *Brachypotherium* (node 15; BS = 2): occipital condyle without a median ridge, mandibular
849 symphysis very massive, labial cingulum usually present on upper premolars and always
850 present on upper molars, lower cheek teeth with a flat ectolophid, lower premolars with a
851 lingual opening of the posterior valley U-shaped, p2 with a paraconid reduced, radius-ulna
852 with a second distal articulation, pyramidal with a distal semilunate-facet asymmetric,
853 posterior facet always absent on the McII-McIII, and fibula-facet oblique on the astragalus.
854 The Bremer Support is low, due to an alternative topology with *B. perimense* being sister
855 taxon to the (*B. brachypus*, node 16) clade appearing at 1317 steps. *Brachypotherium*
856 *brachypus* is particularly well differentiated, with 27 unambiguous cranio-mandibular, dental,
857 and postcranial autapomorphies each (see Table 6). From node 16 diverge two clades, with
858 (*Teleoceras* plus *Prosantorhinus*) on the one hand (node 17), and all species classically

859 assigned to *Diaceratherium* except the type species (node 20). Node 16 (BS = 2) is supported
860 by eight cranio-dental and postcranial unambiguous synapomorphies: vomer rounded,
861 protocone constriction usually absent on P3-4, antecrochet always present on P4, lingual
862 cingulum always present on lower premolars, pyramidal- and McV-facets always separate on
863 the unciform, McIV with a trapezoid outline in proximal view, calcaneus-facets 2 and 3
864 always independent on the astragalus, and fibula-facet always present on the calcaneus. Node
865 17 (BS = 4) places the highly-divergent *Teleoceras fossiger* (39 cranio-mandibular, dental,
866 and postcranial unambiguous autapomorphies; Table 6) as sister species to *Prosantorhinus*,
867 through 14 cranio-mandibular, dental, and postcranial synapomorphies: base of the processus
868 zygomaticus maxillary low on the maxilla, zygomatic arch high, articular tubercle of the
869 squamosal concave, lingual groove (sulcus mylohyoideus) absent on the corpus mandibulae,
870 metaloph transverse and protoloph sometimes interrupted on P2, mesostyle present on M2, d2
871 with a posterior valley usually open, scapula spatulated and with a medial border straight on
872 the glenoid fossa, a trochanter major low on the femur, MtII-facet always absent and cuboid-
873 facet present on the MtIII, and metapodials with high and acute intermediate reliefs.
874 *Prosantorhinus* (node 18; BS = 4) is monophyletic, with *P. germanicus* (thirteen cranio-dental
875 unambiguous autapomorphies; Table 6) as the first offshoot (node 18) and *P. laubei* and *P.*
876 *douvillei* being sister species (node 19). The monophyly of *Prosantorhinus* is supported by
877 seven cranio-dental unambiguous synapomorphies, some being optimised in *P. laubei* (no
878 cranial remains available; Heissig & Fejfar, 2007): lateral apophysis present on the nasals,
879 median nasal horn present (probably in males), presence of a sagittal fronto-parietal crest, of a
880 posterior groove on the processus zygomaticus of the squamosal, of a metacone fold on M1-2,
881 of an unconstricted metaloph on M1, and of an ectolophid fold on d2-3. *Prosantorhinus*
882 *douvillei* (nine unambiguous dental autapomorphies; Table 6) and *P. laubei* (six unambiguous
883 dental autapomorphies; Table 6) share six dental and postcranial unambiguous

884 synapomorphies (node 19; BS = 4): protocone unconstricted on P3-4 and M3, metaloph
885 unconstricted on M2, labial cingulum always present on lower molars, lingual groove always
886 present on d3, and expansion of the calcaneus-facet 1 always high and narrow on the
887 astragalus.

888 Node 20 (BS = 3) gathers eight terminal taxa (Fig. 13). It is supported by ten cranio-
889 dental and postcranial synapomorphies: nuchal tubercle small, articular tubercle smooth on
890 the squamosal, cement present on cheek teeth, protocone always constricted on P3-4, labial
891 cingulum usually absent on lower premolars and always present on lower molars, foramen
892 vertebrale lateralis present and axis-facets transversally concave on the atlas, postero-distal
893 apophysis low on the tibia, and latero-distal gutter located posteriorly on the fibula. Two
894 clades diverge from node 20. The first one (node 21, BS = 3) gathers *Brachydiceratherium*
895 *shanwangense*, *Bd. aginense*, and *Bd. intermedium*, based on eight dental and postcranial
896 synapomorphies: I1 with an oval occlusal outline, labial cingulum always absent on upper
897 premolars, crista usually present on P3, scapula elongated, fossa olecrani high on the
898 humerus, fovea capitis low and wide on the femur, latero-distal gutter deep on the fibula,
899 limbs slender, and insertions for the m. interossei long on lateral metapodials. Most of them
900 are optimised in *Bd. intermedium*. *Brachydiceratherium shanwangense* is well diagnosed,
901 with sixteen cranio-dental and postcranial unambiguous synapomorphies: lateral apophysis
902 present on the nasals, median nasal horn present on the nasals, premolar series short with
903 respect to the molar series, roots distinct on the cheek teeth, crochet always simple and lingual
904 cingulum usually absent and always reduced on P2-4, crista always present on P3, protocone
905 strongly constricted on M1-2, lingual cingulum usually absent on lower premolars and always
906 absent on lower molars, d1/p1 absent in adults, glenoid fossa with a medial border straight on
907 the scapula, distal gutter absent on the lateral epicondyle of the humerus, proximal radius-ulna
908 facets always fused, and trochanter major low on the femur. Node 22 (BS = 3) is supported by

909 five dental and postcranial unambiguous synapomorphies: metaloph short on M1-2, posterior
910 height exceeding the anterior height on the scaphoid, astragalus almost as high as wide (TD/H
911 ratio between 1 and 1.2), and tibia- and fibula-facets absent on the calcaneus.

912 *Brachydiceratherium intermedium* (five dental and postcranial unambiguous autapomorphies;
913 Table 6) is less derived than *Bd. aginense* (16 dental and postcranial unambiguous
914 autapomorphies; Table 6), which probably reflects the strong contrast in the completeness of
915 their hypodigms (e.g., no indisputable cranial remains are documented for *Bd. intermedium*).

916 The second clade diverging from the node 20 (i.e., node 23) places *Bd. fatehjangense* as
917 a sister taxon to (*Bd. aurelianense*, (*Bd. lamilloquense*, (*Bd. lemanense*, *Bd. asphaltense*))).

918 All the corresponding nodes are weakly supported ($1 \leq BS \leq 3$), with low numbers of
919 unambiguous synapomorphies (ranging from three to six). Node 23 is the least-supported one
920 (BS = 1), with five dental and postcranial synapomorphies (metacone fold present on M1-2,
921 second distal radius-ulna articulation present, posterior expansion of the scaphoid-facet low
922 on the radius, postero-proximal semilunate-facet usually absent on the scaphoid, and
923 expansion of the calcaneus-facet 1 usually wide and low on the astragalus).

924 DISCUSSION

925 **Ontogenetic age and sex**

926 Both the complete dental eruption and the wear stages of upper and lower teeth concur
927 to consider this individual as an adult, most likely ~7-15 years old (with reference to recent
928 rhinos; e.g., Hillman-Smith et al., 1986; Hullot et al., 2020). In the absence of I1s (usually
929 highly dimorphic in teleoceratines; see Antoine, 2002 regarding *Prosantorhinus douvillei*),
930 and due to the fragmentary state of i2s, it is not possible to determine its sex.

931 **Taxonomic inferences**

932 Surprisingly, *Diaceratherium tomerdingense* Dietrich, 1931 is retrieved as the first
933 offshoot among Teleoceratina (Fig. 13). Moreover, the assignment of this hornless and robust-
934 limbed rhinocerotine to the subtribe is not well supported at all (BS = 1): in other words, this
935 species could be closely related to Rhinocerotina instead among Rhinocerotini, as suggested
936 by some of its peculiar features, retrieved as autapomorphies in the current analysis (metaloph
937 short on M1-2; distal gutter on the lateral epicondyle absent on the humerus, distal border of
938 the anterior side of the semilunate rounded, and trapezium-facet absent on the McII).
939 Accordingly, and taking into account both the topology of the most parsimonious tree and the
940 character distribution along its branches, we propose that *Diaceratherium* Dietrich, 1931 shall
941 be restricted to the type species.

942 Indeed, all other species previously assigned to *Diaceratherium* in the last decades form
943 a well-supported clade remote from the type species (Fig. 13). This clade is split into two
944 sister clades encompassing three and five species, respectively (*D. shanwangense*, *D.*
945 *aginense*, and *D. intermedium*; *D. fatehjangense*, *D. aurelianense*, *D. lamilloquense*, *D.*
946 *asphaltense*, and *D. lemanense*). Except for *D. lamilloquense* Michel, 1987, these species
947 were originally or subsequently assigned to pre-existing genera, i) either unambiguously non-
948 related to Teleoceratina, such as *Aceratherium* (*D. lemanense*), *Diceratherium* (*D.*
949 *asphaltense*, *D. lemanense*), *Aprotodon* (*D. fatehjangense*), *Chilotherium* or *Subchilotherium*
950 (*D. intermedium*), and *Plesiaceratherium* (*D. shanwangense*), or ii) among Teleoceratina,
951 with *Teleoceras* and/or *Brachypotherium* (*D. aginense*, *D. aurelianense*, *D. shanwangense*,
952 and *D. fatehjangense*). Finally, and to our knowledge, the only species belonging to this clade
953 for which a genus-group name has been unambiguously proposed is *D. lemanense*. Indeed,
954 Lavocat (1951) has erected the subgenus *Brachydiceratherium* for “*Acerotherium lemanense*
955 Pomel, 1853”. Interestingly, Lavocat did assign these species and subgenus to *Diceratherium*
956 Marsh, 1875, a genus consistently assigned to Elasmotheriinae in the last decades (e.g.,

957 Antoine, 2002). We propose that all these eight species be assigned to *Brachydiceratherium*
958 Lavocat, 1951, especially as the five-species clade, with *D. fatehjangense*, *D. aurelianense*,
959 *D. lamilloquense*, *D. asphaltense*, and *D. lemanense*, is not well supported (BS = 1; 5
960 unambiguous synapomorphies). Noteworthy, *D. asphaltense* and *D. lemanense* are sister
961 species in the most parsimonious tree, with a low number of morpho-anatomical
962 discrepancies. It should be noted that Jame et al. (2019) consider both species as being
963 distinct, based on a wide array of cranio-dental and postcranial features.

964 Other teleoceratine genera are monophyletic in the present analysis. *Brachypotherium*
965 Roger, 1904 includes *B. brachypus* and *B. perimense* and this genus is a sister group to a
966 clade gathering *Teleoceras* Hatcher, 1894 plus *Prosantorhinus* Heissig, 1974 on one branch
967 and *Brachydiceratherium* on the other one (see above).

968 **Historical biogeography of Eurasian teleoceratines**

969 During early Miocene times, Teleoceratina were particularly species-rich in Eurasia,
970 with 5–8 coeval species in any time slices (Fig. 14). A common thread between
971 *Brachypotherium*, *Brachydiceratherium*, and *Prosantorhinus* is their huge geographical range
972 at the generic level, encompassing most of the Eurasian landmasses for the latter two genera
973 (e.g., Heissig, 1999; Antoine et al., 2010, 2013), plus Afro-Arabia for *Brachypotherium* (e.g.,
974 Hooijer, 1963, Geraads & Miller, 2013; Pandolfi & Rook, 2019). An early representative of
975 *Brachydiceratherium* has been recognised in Thailand (*Bd. cf. lamilloquense*; Marivaux et al.,
976 2004). It has the closest affinities with *Bd. lamilloquense*, from the late Oligocene of Western
977 Europe (Fig. 15). To our knowledge, no occurrence has been reported between both areas for
978 this species. *Prosantorhinus* has a similar geographical range, extending from Western
979 Europe (*P. germanicus* and *P. douvillei*; Heissig, 1972b; Antoine et al., 2000; Heissig, 2017)
980 and Central Europe (*P. laubei*; Heissig & Fejfar, 2007) to Southern Pakistan (*P. shahbazi*;
981 Antoine et al., 2010, 2013). If confirmed, the recognition of *Bd. fatehjangense* in lower

982 Miocene beds of the Turgai region in Kazakhstan, previously described as a representative of
983 *Bd. aurelianense* by Borissiak (1927) and Lu et al. (2021), would considerably expand
984 latitudinally the range of this species, previously restricted to the Indian Subcontinent. It
985 would then be documented on both sides of the Himalayas (Fig. 15). The ubiquitous
986 distributions of most teleoceratine taxa likely underline ultra-generalist ecological preferences
987 (Hullot et al., 2021). Moreover, such ranges seemingly support the absence of efficient
988 ecological and geographical barriers at the Eurasian scale for the concerned teleoceratines, at
989 least by early Miocene times (Fig. 15).

990 Moreover, ghost lineages within *Brachypotherium* and *Prosantorhinus* (Fig. 14) are
991 likely to be bridged by *B. gajense* and *P. shahbazi*, from the latest Oligocene–earliest
992 Miocene and the early Miocene of Pakistan, respectively (for further discussion, see Antoine
993 et al., 2013 and Antoine, in press).

994 *Brachydiceratherium shanwangense* was previously only documented at Shanwang,
995 eastern China (N32°, E116.5°). The well-supported specific assignment of the Tagay
996 rhinoceros (N53°, E107.5°) points to an unsuspectedly wide geographical range for this
997 species, further pleading for both a low climatic and environmental gradient in the concerned
998 area at that time and very broad ecological preferences for this species (Fig. 15). Moreover, it
999 can be suspected that the smallest teleoceratine remains described over the early Miocene
1000 interval in Japan (Kani and Mizunami formations) and referred to the *Brachypotherium*
1001 *pugnator* (Matsumoto, 1921), otherwise of gigantic dimensions (Fukuchi & Kawai, 2011;
1002 Tomida et al., 2013; Handa, 2020), may have particularly close affinities with those of *Bd.*
1003 *shanwangense*. More generally, the concerned Japanese assemblages are very similar to the
1004 Tagay and Shanwang ones (e.g., with the equid *Anchitherium* cf. *gobiense*, the proboscidean
1005 *Gomphotherium annectens*, and the beaver *Youngofiber sinensis*; Qiu & Qiu, 2013), thus
1006 strengthening the existence of a single eastern Asian biogeographical province at mid

1007 latitudes at that time (Fig. 15). Indeed, closed forest environments under a subtropical climate,
1008 with precipitation averaging ca. 1500 mm per year, are reported for the Shanwang Basin
1009 based on early Miocene floras and vertebrates (Lu et al., 2021). The same proxies allow for
1010 considering the Tagay area as a lake, also surrounded by dense forests under subtropical
1011 conditions, with precipitation averaging ca. 1000-1500 mm per year (Logachev et al, 1964;
1012 Belova, 1985; Sizov & Klementiev, 2015).

1013 CONCLUSIONS

1014 The numerous associated features documented and scored in the Tagay rhinocerotid
1015 skeleton have allowed for assigning it to the same teleoceratine species (*Brachydiceratherium*
1016 *shanwangense*) as in Shanwang, eastern China. These remains further contribute to a refined
1017 depiction of phylogenetic relationships and to a revision of generic assignments among
1018 Eurasian Teleoceratina.

1019 The genus *Diaceratherium* Dietrich, 1931 should be restricted to the type species,
1020 *Diaceratherium tomerdingense* Dietrich, 1931. This monotypic genus is the first offshoot
1021 within Teleoceratina. Our results support the reappraisal of *Brachydiceratherium* Lavocat,
1022 1951, with eight assigned species: *Brachydiceratherium lemanense* (Pomel, 1853),
1023 *Brachydiceratherium aurelianense* (Nouel, 1866), *Brachydiceratherium intermedium*
1024 (Lydekker, 1884), *Brachydiceratherium asphaltense* (Depéret & Douxami, 1902),
1025 *Brachydiceratherium fatehjangense* (Pilgrim, 1910), *Brachydiceratherium aginense* (Répelin,
1026 1917), *Brachydiceratherium shanwangense* (Wang, 1965) and *Brachydiceratherium*
1027 *lamilloquense* Michel, 1983. *Brachydiceratherium* is a sister group to a clade encompassing
1028 *Prosantorhinus* and the North American genus *Teleoceras*. *Brachypotherium* is more closely
1029 related to the latter three genera than to *Diaceratherium*.

1030 All Old World teleoceratines have extended geographical distributions at the genus
1031 level, which is also true for some species, such as the late Oligocene *Brachydiceratherium*
1032 *lamilloquense* and the early Miocene *Brachydiceratherium shanwangense*. The latter range
1033 supports the existence of a single eastern Asian biogeographical province at mid latitudes at
1034 that time for such megaherbivores.

1035 ACKNOWLEDGMENTS

1036 We are grateful to our colleagues for having participated in the 2008-2021 excavations.
1037 Special thanks to Gennady Turkin for logistical support and for assistance in the field. Valeria
1038 Burova and Ekaterina Nikulina are acknowledged for working on the skeleton reconstruction.
1039 Géraldine Véron and Christine Argot (Muséum National d'Histoire Naturelle (Paris, France)
1040 kindly provided access to zoological and paleontological collections under their care. We
1041 deeply acknowledge the Recommender, Faysal Bibi, and all three reviewers (Jérémy Tissier,
1042 Deng Tao, and Panagiotis Kampouridis), for their thorough revisions and constructive
1043 remarks on a widely-improvable previous version of the manuscript.

1044 FUNDING

1045 The work related to the study of the geological structure of the section was supported by
1046 the Russian Foundation for Basic Research, project numbers 22-17-00049 «Neotectonics and
1047 active tectonics of the northern part of Central Asia».

1048 REFERENCES

1049 **Antoine P-O. 2002.** Phylogénie et évolution des Elasmotheriina (Mammalia,
1050 Rhinocerotidae). *Mémoires du Muséum National d'Histoire Naturelle* **188**: 1–359.

1051 **Antoine P-O. in press.** Rhinocerotids from the Siwalik faunal sequence. In: Badgley, C.,
1052 Pilbeam, D. & Morgan, M. (Eds.), *At the Foot of the Himalayas: Paleontology and*
1053 *Ecosystem Dynamics of the Siwalik Record of Pakistan*. Johns Hopkins University Press.

1054 **Antoine P-O, Welcomme J-L. 2000.** A new rhinoceros from the Bugti Hills, Baluchistan,
1055 Pakistan: the earliest elasmotheriine. *Palaeontology* **43**: 795–816.

1056 **Antoine P-O, Fleury G, Duranthon F. 2002.** Le rhinocérotidé *Prosantorhinus douvillei*
1057 (Osborn, 1900) de l'Orléanien supérieur de Captieux (Gironde). *Bulletin de la Société*
1058 *d'Histoire Naturelle de Toulouse* **137**: 87–91.

1059 **Antoine P-O, Duranthon F, Welcomme J-L. 2003.** *Alicornops* (Mammalia, Rhinocerotidae)
1060 dans le Miocène supérieur des Collines Bugti (Balouchistan, Pakistan): implications
1061 phylogénétiques. *Geodiversitas* **25**: 575–603.

1062 **Antoine P-O, Ducrocq S, Marivaux L, Chaimanee Y, Crochet J-Y, Jaeger J-J,**
1063 **Welcomme J-L. 2003.** Early rhinocerotids (Mammalia: Perissodactyla) from South Asia
1064 and a review of the Holartic Paleogene rhinocerotid record. *Canadian Journal of Earth*
1065 *Sciences* **40**: 365–374.

1066 **Antoine P-O, Downing KF, Crochet J-Y, Duranthon F, Flynn LJ, Marivaux L, Métais**
1067 **G, Rajpar AR, Roohi G. 2010.** A revision of *Aceratherium blanfordi* Lydekker, 1884
1068 (Mammalia: Rhinocerotidae) from the Early Miocene of Pakistan: postcranials as a key.
1069 *Zoological Journal of the Linnean Society* **160**: 139–194.

1070 **Antoine P-O, Becker D. 2013.** A brief review of Agenian rhinocerotids in Western Europe.
1071 *Swiss Journal of Geosciences* **106**: 135–146.

1072 **Antoine P-O, Becker D, Laurent Y, Duranthon F. 2018.** The Early Miocene teleoceratine
1073 *Prosantorhinus* aff. *douvillei* (Mammalia, Perissodactyla, Rhinocerotidae) from Béon 2,
1074 Southwestern France. *Revue de Paléobiologie* **37**: 367–377.

1075 **Antoine P-O, Becker D, Pandolfi L, Geraads D. accepted.** Evolution and fossil record of
1076 Old World Rhinocerotidae. In: Melletti M, Balfour D, Talukdar B. (Eds.), *Rhinos of the*
1077 *World: Ecology, Conservation and Management*. Fascinating Life Sciences, Springer
1078 Nature.

1079 **Antoine P-O, Métais G, Orliac MJ, Crochet J-Y, Flynn LJ, Marivaux L, Rajpar AR,**
1080 **Roohi G., Welcomme J-L. 2013.** Mammalian Neogene biostratigraphy of the Sulaiman
1081 Province, Pakistan. In: Wang X-m, Flynn LJ, Fortelius M (eds.), *Fossil mammals of Asia:*
1082 *Neogene Biostratigraphy and Chronology*, Columbia University Press 400–422.

1083 **Antoine P-O, Reyes MC, Amano N, Bautista AP, Chang CH, Claude J, Vos JD, Ingicco**
1084 **T. 2022.** A new rhinoceros clade from the Pleistocene of Asia sheds light on mammal
1085 dispersals to the Philippines. *Zoological Journal of the Linnean Society* **194**: 416–430.
1086 DOI: 10.1093/zoolinnean/zlab009

1087 **Becker D, Antoine P-O, Maridet O. 2013.** A new genus of Rhinocerotidae (Mammalia,
1088 Perissodactyla) from the Oligocene of Europe. *Journal of Systematic Palaeontology* **11**:
1089 947-972.

1090 **Belova VA. 1985.** *Vegetation and climate of the Late Cenozoic of the south of Eastern*
1091 *Siberia*. Novosibirsk: Nauka [in Russian].

1092 **Boada-Saña A. 2008.** *Phylogénie du rhinocérotyde Diaceratherium Dietrich, 1931*
1093 *(Mammalia, Perissodactyla)*. Master thesis dissertation. University of Montpellier,
1094 France, 2.

1095 **Boivin M, Marivaux L, Antoine P-O. 2019.** L’apport du registre paléogène d’Amazonie sur
1096 la diversification initiale des Caviomorpha (Hystricognathi, Rodentia) : implications
1097 phylogénétiques, macroévolutives et paléobiogéographiques. *Geodiversitas* **41**: 143–245.

1098 **Borissiak A. 1914.** On the dental apparatus of *Elasmotherium caucasicum* n. sp. *Bulletin de*
1099 *l’Académie Impériale des Sciences de St-Petersbourg* **6**: 555–584.

- 1100 **Borissiak A. 1927.** *Brachypotherium aurelianense* Nouel, var. nov. Gailiti, from the Miocene
1101 deposits of the Turgai region. *Bulletin de l'Académie des Sciences de l'URSS* **21**: 273–
1102 286.
- 1103 **Bremer KR. 1994.** Branch support and tree stability. *Cladistics* **10**: 295–304.
- 1104 **Burchell WJ. 1817.** Note sur une nouvelle espèce de Rhinoceros. *Bulletin de la Société*
1105 *Philomathique de Paris (June)*.
- 1106 **Cerdeño E. 1993.** Étude sur *Diaceratherium aurelianense* et *Brachypotherium brachypus*
1107 (Rhinocerotidae, Mammalia) du Miocène moyen de France. *Bulletin du Muséum national*
1108 *d'Histoire naturelle* **15**: 25–77.
- 1109 **Cerdeño E. 1995.** Cladistic analysis of the Family Rhinocerotidae (Perissodactyla). *American*
1110 *Museum Novitates* **3143**: 1–25.
- 1111 **Crusafont M, Villalta JF, Truyols J. 1955.** El Burdigaliense continental de la Cuenca del
1112 Vallés-Penedés. *Memorias y Comunicaciones del Instituto Geológico, Barcelona* **12**: 1–
1113 272.
- 1114 **Danilov IG, Syromyatnikova EV, Klementiev AM, Sizov AV, Martynovich NV,**
1115 **Zelenkov NV, Sychevskaya EK, Tesakov AS. 2012.** New data on Miocene vertebrates
1116 of Tagay locality (Olkhon, Lake Baikal). In: Lopatin AV, Parkhaev PYu, Rozanov AYu
1117 eds. *Modern Paleontology: classical and new methods. The ninth all-Russian scientific*
1118 *school for young scientists in Paleontology*. Moscow: Paleontological Institute 19–20 [in
1119 Russian].
- 1120 **Daxner-Höck G, Böhme M, Kossler A. 2013.** New Data on Miocene Biostratigraphy and
1121 Paleoclimatology of Olkhon Island (Lake Baikal, Siberia). In: Wang X, Flynn LJ,
1122 Fortelius M, eds., *Fossil mammals of Asia: Neogene biostratigraphy and chronology*,
1123 New York: Columbia University Press, 508-517.

- 1124 **Daxner-Höck G, Mörs T, Kazansky AY, Matasova GG, Ivanova VV, Shchetnikov AA,**
1125 **Filinov IA, Voyta L, Erbajeva MA, 2022.** A synthesis of fauna, palaeoenvironments
1126 and stratigraphy of the Miocene Tagay locality (Olkhon Island, Lake Baikal, Eastern
1127 Siberia). *Palaeobio Palaeoenv* **102**, 969–983.
- 1128 **Deng T, Gao F. 2006.** Perissodactyla. In: Qi GQ, Dong W (Eds). *Lufengpithecus hudienensis*
1129 *site*. Beijing: Science Press, 188–195 (in Chinese), 334–335 (in English).
- 1130 **Depéret C, Douxami H. 1902.** Les Vertébrés oligocènes de Pyrimont-Challonges (Savoie).
1131 *Mémoires suisses de Paléontologie* **29**: 1–92.
- 1132 **Dietrich WO. 1931.** Neue Nashornreste aus Schwaben (*Diaceratherium tomerdingensis* n. g.
1133 n. sp.). *Zeitschrift für Säugetierkunde* **6**: 201–223.
- 1134 **Falconer H, Cautley PT. 1847.** *Fauna antiqua Sivalensis, being the fossil zoology of the*
1135 *Sewalik Hills, in the North of India (Sus, Rhinoceros, Chalicotherium)*. London: Smith,
1136 Elder and Co..
- 1137 **Filippov AG, Sytchevskaya EK. 2000.** Remains of snakeheaded fishes (Channidae) near
1138 Lake Baikal. *The Third Vereshchagin Baikal Conference, Aug 22-27, Irkutsk*, 251.
- 1139 **Fischer von Waldheim GF. 1814.** *Zoögnosia tabulis synopticis illustrate, in usum*
1140 *Paeselectionum Academiae Imperialis Medicochirurgae*. Moscow: Nicolai Sergeidis
1141 Vsevolozsky.
- 1142 **Fukuchi A, Kawai K. 2011.** Revision of fossil rhinoceroses from the Miocene Mizunami
1143 Group, Japan. *Palaeontological Research* **15**: 247–257.
- 1144 **Geraads D. 2010.** Rhinocerotidae. In: Werdelin L, Sanders WJ (Eds.), *Cenozoic Mammals of*
1145 *Africa*. University of California Press, Berkeley, 675–689.
- 1146 **Geraads D, Miller E. 2013.** *Brachypotherium minor* n. sp., and other Rhinocerotidae from
1147 the Early Miocene of Buluk. Northern Kenya. *Geodiversitas* **35**: 359–375. DOI:
1148 10.5252/g2013n2a5.

- 1149 **Guérin C. 1980.** Les rhinocéros (Mammalia, Perissodactyla) du Miocène terminal au
1150 Pléistocène supérieur en Europe occidentale. Comparaison avec les espèces actuelles.
1151 *Documents des Laboratoires de Géologie de Lyon* **79**: 1–1185.
- 1152 **Handa N. 2020.** Reappraisal of a rhinocerotid (Mammalia, Perissodactyla) from the lower
1153 Miocene Yotsuyaku Formation, Northeast Japan, with an overview of the early Miocene
1154 Japanese rhinocerotids. *Paleontological Research* **24**: 183–191.
- 1155 **Heissig K. 1969.** Die Rhinocerotidae (Mammalia) aus der oberoligozänen Spaltenfüllung von
1156 Gaimersheim bei Ingolstadt in Bayern und ihre phylogenetische Stellung. *Verlag der*
1157 *Bayerischen Akademie der Wissenschaften* **138**: 1–133.
- 1158 **Heissig K. 1972a.** Paläontologische und geologische Untersuchungen im Tertiär von
1159 Pakistan. 5 – Rhinocerotidae (Mamm.) aus den unteren und mittleren Siwalik-schichten.
1160 *Abhandlungen der Bayerischen Akademie der Wissenschaften, München, mathematische-*
1161 *naturwissenschaftliche Klasse* **152**: 1–112.
- 1162 **Heissig K. 1972b.** Die obermiozäne Fossil-Lagerstätte Sandelzhausen. 5. Rhinocerotidae
1163 (Mammalia), Systematik und Ökologie. *Mitteilungen der Bayerischen Staatssammlung*
1164 *für Paläontologie und historische Geologie* **12**: 57–81.
- 1165 **Heissig K. 1999.** Family Rhinocerotidae. In: Rössner GE, Heissig K. eds. *The Miocene Land*
1166 *Mammals of Europe*. Dr Pfeil, Munich 175–188.
- 1167 **Heissig K, Fejfar O. 2007.** Die fossilen Nashörner (Mammalia, Rhinocerotidae) aus dem
1168 Untermiozän von Tuchořice in Nordwestboehmen. *Acta Musei Nationalis Pragae B* **63**:
1169 19-64.
- 1170 **Heissig K. 2012.** Les Rhinocerotidae (Perissodactyla) de Sansan. *Mémoires du Muséum*
1171 *national d'Histoire naturelle de Paris* **203**: 317–485.

1172 **Heissig K. 2017.** Revision of the European species of *Prosantorhinus* Heissig, 1974
1173 (Mammalia, Perissodactyla, Rhinocerotidae). *Fossil Imprint* **122**: 265–294. DOI :
1174 10.1515/if-2017-0014.

1175 **Hilgen FJ, Lourense LJ, Van Dam JA. 2012.** The Neogene period. In: Gradstein FM, Ogg
1176 JG, Schmitz MD, Ogg GM, eds. *The Geologic Time Scale 2012*. Oxford: Elsevier 923–
1177 978.

1178 **Hooijer DA. 1963.** Miocene Mammalia of the Congo. *Musée royal de l’Afrique Centrale.*
1179 *Annales - sciences géologiques* **46**: 1–77.

1180 **Hullot M, Laurent Y, Merceron G, Antoine P-O. 2021.** Paleoecology of the
1181 Rhinocerotidae (Mammalia, Perissodactyla) from Béon 1, Montréal-du-Gers (late early
1182 Miocene, SW France): Insights from dental microwear texture analysis, mesowear, and
1183 enamel hypoplasia. *Palaeontologia Electronica* **24**: a27. DOI: 10.26879/1163

1184 **Jame C, Tissier J, Maridet O, Becker D 2019.** Early Agenian rhinocerotids from Wischberg
1185 (Canton Bern, Switzerland) and clarification of the systematics of the genus
1186 *Diaceratherium*. *PeerJ* **7**: e7517.

1187 **Kitainik AF, Ivaniev LN. 1958.** A note on the Tertiary deposits of Olkhon Island on Lake
1188 Baikal. *Notes of the Irkutsk Regional Museum of Local History* 55–60.

1189 **Klementiev AM. 2009.** Finding a Miocene rhinoceros on Olkhon Island (Lake Baikal). In:
1190 Barskov IS & Nazarova VM eds. *200 years of national paleontology. Materials of the*
1191 *All-Russian meeting*. Moscow: Paleontological Institute, 56–57 [in Russian].

1192 **Klementiev AM, Sizov AV. 2015.** New record of anchithere (*Anchitherium aurelianense*) in
1193 the Miocene of Eastern Siberia, Russia. *Russian Journal of Theriology* **14**: 133-143.

1194 **Kossler A. 2003.** Neogene sediments of Olkhon and Svyatoy Nos (Baikal Rift System, East
1195 Siberia): Suggestions about the development of Lake Baikal. *Berliner Paläobiologische*
1196 *Abhandlungen* **4**: 55–63.

- 1197 **Khan MA, Akhtar M, Khan AM, Ghaffar A, Iqbal M, Samiullah K. 2011.** New fossil
1198 locality in the Middle Miocene of Lava from the Chinji Formation of the Lower Siwaliks,
1199 Pakistan. *Pakistan Journal of Zoology* **43**: 61–72
- 1200 **Khosatzky LI, Chkhikvadze VM. 1993.** New data about Miocene turtles of the genus
1201 *Baicalemys*. *Bulletin of the Academy of Science of Georgia* **148**: 155–160 [in Russian].
- 1202 **von Koenigswald GHR. 1956.** Fossil Mammals from the Philippines. *National Research*
1203 *Council of the Philippines, University of the Philippines Diliman. Special reprint. Full*
1204 *text illustrations of paper 22 Proceedings of the Fourth Far-Eastern Prehistory*
1205 *Congress*: 1–14.
- 1206 **Kordikova EG. 2001.** Remarks on the Oligocene-Miocene mammal paleontology and
1207 sequence stratigraphy of South-Western Betpakdala Steppe, South Kazakhstan. *Neues*
1208 *Jahrbuch für Geologie und Paläontologie Abhandlungen* **221**: 35–79.
- 1209 **Lartet E. 1851.** *Notice sur la colline de Sansan*. Auch: Portes.
- 1210 **Laurillard F. 1848.** Rhinocéros fossiles, in d’Orbigny CD (ed.), *Dictionnaire universel*
1211 *d’Histoire naturelle*, volume 11. Renard, Martinet & Cie, Paris: 99–102.
- 1212 **Linnaeus C. 1758.** *Systema Naturae per regna tria naturae, secundum classes, ordines,*
1213 *genera, species, cum characteribus, differentiis, synonymis, locis*. Vol. 1. Tenth Edition.
1214 Stockholm: Regnum animale.
- 1215 **Logachev NA, Lomonosova TK, Klimanova VM. 1964.** *The Cenozoic deposits of the*
1216 *Irkutsk amphitheatre*. Moscow: Nauka [in Russian].
- 1217 **Lavocat R. 1951.** *Révision de la faune des mammifères oligocènes d’Auvergne et du Velay*.
1218 Sciences et Avenir, Paris.
- 1219 **Lu X, Cerdeño E, Zheng X, Wang S, Deng T. 2021.** The first Asian skeleton of
1220 *Diaceratherium* from the early Miocene Shanwang Basin (Shandong, China), and
1221 implications for its migration route. *Journal of Asian Earth Sciences: X* **6**: 100074

- 1222 **Lydekker R. 1884.** Additional Siwalik Perissodactyla and Proboscidea. *Memoirs of the*
1223 *Geological Survey of India – Palaeontologia Indica* **3**: 1–34.
- 1224 **MacFadden BJ. 1998.** Equidae, In: Janis CM, Scott KM, Louis LL eds. *Evolution of Tertiary*
1225 *Mammals North America*. vol. 1. Cambridge University Press 537–559.
- 1226 **Marivaux L, Chaimanee Y, Yamee C, Srisuk P, Jaeger J-J. 2004.** Discovery of *Fallomus*
1227 *ladakhensis* Nanda & Sahni, 1998 (Mammalia, Rodentia, Diatomyidae) in the lignites of
1228 Nong Ya Plong (Phetchaburi Province, Thailand): systematic, biochronological and
1229 paleoenvironmental implications. *Geodiversitas*, **26**: 493-507.
- 1230 **Mats VD, Ufimtsev GF, Mandelbaum MM., Alakshin AM, Pospeev AV, Shimaraev MN,**
1231 **Khlystov OM. 2001.** *Cenozoic of the Baikal rift zone*. Novosibirsk: GEO SO RAS Press
1232 [in Russian].
- 1233 **Mats VD, Lomonosova TK, Vorobyeva GA, Vologina EG. 2010.** Late Cretaceous-
1234 Cenozoic sediments of the Baikal rift basin and changing natural conditions.
1235 *Geodynamics & Tectonophysics* **1**: 75–86 [in Russian].
- 1236 **Mats VD, Yefimova IM. 2011.** Paleogeographic scenario of the Late Cretaceous – Cenozoic
1237 for the central part of the Baikal region. *Geodynamics & Tectonophysics* **2**: 175–193 [in
1238 Russian].
- 1239 **Mats VD. 2013.** Late Cretaceous and Cenozoic Stratigraphy of the Baikal Rift Sediments.
1240 *Stratigraphy and Geological Correlation* **21**: 637–651. DOI:
1241 10.1134/S0869593813060075
- 1242 **Mats VD. 2015.** The Baikal rift: Pliocene (Miocene) – Quaternary episode or product of
1243 extended development since the Late Cretaceous under various tectonic factors. A
1244 review. *Geodynamics & Tectonophysics* **6**: 467–489 [in Russian]. DOI: 10.5800/GT-
1245 2015-6-4-0190

- 1246 **Matsumoto H. 1921.** Descriptions of some new fossil mammals from Kani District, Province
1247 of Mino, with revisions of some Asiatic fossil rhinocerotids. *The Science Reports of the*
1248 *Tohoku Imperial University. Second Series (Geology)* **5**: 75–91.
- 1249 **Ménouret B, Guérin C. 2009.** *Diaceratherium massiliae* nov. sp. from the Oligocene clays
1250 of Saint-André and Saint-Henri in Marseille and Les Milles near Aix-en-Provence (South
1251 Eastern France), the first European large brachypod Rhinocerotidae. *Geobios* **42**: 293–
1252 327.
- 1253 **Noel E. 1866.** Mémoire sur un nouveau rhinocéros fossile. Mémoires de la Société
1254 d’Agriculture, Sciences, *Belle-Lettres et Art d’Orléans* **8**: 241–251.
- 1255 **Orliac MJ, Antoine P-O, Ducrocq S. 2010.** Phylogenetic relationships of the Suidae
1256 (Mammalia, Cetartiodactyla): new insights on the relations within Suoidea. *Zoologica*
1257 *Scripta* **39**: 315–330.
- 1258 **Osborn HF. 1900.** Phylogeny of the rhinoceroses of Europe. *Memoirs of the American*
1259 *Museum of Natural History* **13**: 229–267.
- 1260 **Pandolfi L, Rook L. 2019.** The latest Miocene Rhinocerotidae from Sahabi (Libya). *Comptes*
1261 *Rendus Palevol* **18**: 442–448. DOI: 10.1016/j.crpv.2019.03.002.
- 1262 **Pandolfi L, Antoine P-O, Bukhsianidze M, Lordkipanidze D, Rook L. 2021.** Northern
1263 Eurasian rhinocerotines (Mammalia, Perissodactyla) by the Pliocene–Pleistocene
1264 transition: phylogeny and historical biogeography. *Journal of Systematic Palaeontology*.
1265 DOI: 10.1080/14772019.2021.1995907
- 1266 **Pilgrim GE. 1910.** Notice on new mammal genera and species from the Tertiaries of India.
1267 *Records of the Geological Survey of India* **15**: 63–71.
- 1268 **Pokatilov AG. 2004.** *Paleontology and stratigraphy of the Cenozoic of the south of Eastern*
1269 *Siberia and adjacent territories*. Irkutsk: Irkutsk State Technical University Press [in
1270 Russian].

- 1271 **Pomel M. 1853.** *Catalogue méthodologique et descriptif des vertébrés fossiles découverts*
1272 *dans le bassin hydrographique supérieur de la Loire, et surtout dans la vallée de son*
1273 *affluent principal, l'Allier.* Paris: Baillière Ed.
- 1274 **Prieto J., Antoine P-O, Böhme M, van der Made J, Métais G, Laq The Phuc, Quý**
1275 **Truong Quan, Schneider S, Dang Ngoc Tran, Vasilyan D, Luong The Viet, 2018.**
1276 Biochronological and paleobiogeographical significance of the earliest Miocene mammal
1277 fauna from Northern Vietnam. *Palaeobiodiversity and Palaeoenvironments* **98**: 287–313.
1278 doi 10.1007/s12549-017-0295-y
- 1279 **Prothero DR, Guérin C, Manning E. 1989.** The History of the Rhinoceroidea. In:
1280 Prothero DR & Schoch RM eds. *The Evolution of Perissodactyls*, New York: Oxford
1281 University Press, 322–340.
- 1282 **Prothero DR. 2005.** *The evolution of North American Rhinoceroses.* Cambridge; New York;
1283 Melbourne: Cambridge University Press.
- 1284 **Qiu ZD, Qiu ZX. 2013.** Early Miocene Xiejiahe and Sihong fossil localities and their faunas,
1285 eastern China. In: Wang X-m, Flynn LJ, Fortelius M (eds.), *Fossil mammals of Asia:*
1286 *Neogene Biostratigraphy and Chronology*, Columbia University Press 142–154.
- 1287 **Raffi I, Wade BS, Pálike H, Beu AG, Cooper R, Crundwell MP, Krijgsman W, Moore T,**
1288 **Raine I, Sardella R, Vernyhorova YV. 2020.** Chapter 29 - The Neogene Period. In:
1289 Gradstein FM, Ogg JG, Schmitz MD, Ogg GM ads. *Geologic Time Scale 2020.* Elsevier
1290 1141–1215. DOI: /10.1016/B978-0-12-824360-2.00029-2.
- 1291 **Rage JC, Danilov IG. 2008.** A new Miocene fauna of snakes from eastern Siberia, Russia.:
1292 Was the snake fauna largely homogenous in Eurasia during the Miocene? *Comptes*
1293 *Rendus Palevol* **7**: 383–390. DOI: 10.1016/j.crpv.2008.05.004.

- 1294 **Répin J. 1917.** Études paléontologiques dans le sud-ouest de la France (Mammifères). Les
1295 rhinocerotidés de l'Aquitainien supérieur de l'Agenais (Laugnac). *Annales du Muséum*
1296 *d'Histoire naturelle de Marseille* **16**: 1–47.
- 1297 **Rössner G.E., Mörs T. 2001.** A New Record of the Enigmatic Eurasian Miocene Ruminant
1298 Artiodactyl *Orygotherium*. *Journal of Vertebrate Paleontology* **21**: 591-595.
- 1299 **Sizov AV, Klementiev AM. 2015.** Geology and taphonomy of Tagay locality of early
1300 Miocene vertebrate fauna. In: Lipnina EA & Berdnikov IM, eds. *Eurasia in the Cenozoic.*
1301 *Stratigraphy, paleoecology, cultures*. Irkutsk: Irkutsk State University Press, 206–218 [in
1302 Russian].
- 1303 **Sotnikova MV, Klementiev AM, Sizov AV, Tesakov AS. 2021.** New species of *Ballusia*
1304 Ginsburg and Morales, 1998 (Ursidae, Carnivora) from Miocene of Eastern Siberia,
1305 Russia. *Historical Biology* **33**: 486-497, DOI: 10.1080/08912963.2019.1637864
- 1306 **Swofford, D.L. 2002.** *PAUP*: Phylogenetic analysis using parsimony (*and other methods).*
1307 *Version 4.0b10*, Sunderland, Sinauer Associates, Inc., Publishers, Sunderland.
- 1308 **Syromyatnikova EV. 2014.** The first record of *Salamandrella* (Caudata: Hynobiidae) from
1309 the Neogene of Russia. *Russian Journal of Herpetology* **21**: 217–220.
- 1310 **Syromyatnikova EV. 2015.** A New Species of *Bufo* (Amphibia, Anura) from the Miocene of
1311 Russia. *Russian Journal of Herpetology* **22**: 281–288.
- 1312 **Tesakov AS, Lopatin AS. 2015.** First record of Mylagaulid rodents (Rodentia, Mammalia)
1313 from the Miocene of Eastern Siberia (Olkhon Island, Baikal Lake, Irkutsk Region,
1314 Russia). *Doklady Biological Sciences* **460**: 23–26.
- 1315 **Tissier J, Antoine P-O, Becker D. 2021.** New species, revision, and phylogeny of
1316 *Ronzotherium* Aymard, 1854 (Perissodactyla, Rhinocerotidae). *European Journal of*
1317 *Taxonomy* **753**: 1–80. DOI: 10.5852/ejt.2021.753.1389

- 1318 **Tissier J, Geiger-Schütz P, Flückiger PF, Becker D. 2021.** Neue Erkenntnisse über die
1319 Nashorn-Funde von Rickenbach (SO) (Oberes Oligozän, Kanton Solthurn, Schweiz) aus
1320 der Sammlung des Naturmuseums Olten. *Naturforschende Gesellschaft des Kantons*
1321 *Solothurn* **44**: 25–50
- 1322 **Tomida Y, Nakaya H, Saegusa H, Miyata K, Fukuchi A. 2013.** Miocene Land Mammals
1323 and Stratigraphy of Japan. In: Wang X, Flynn LJ, Fortelius M, eds., *Fossil mammals of*
1324 *Asia: Neogene biostratigraphy and chronology*, New York: Columbia University Press,
1325 314–333.
- 1326 **Vislobokova IA. 1990.** About artiodactyls from the Lower Miocene of the Tagay bay,
1327 Olkhon island (Baikal). *Paleontological Journal* **2**: 134–138 [in Russian].
- 1328 **Vislobokova IA. 1994.** The Lower Miocene artiodactyls of Tagay Bay, Olkhon Island, Lake
1329 Baikal (Russia). *Palaeovertebrata*. **23**: 177–197.
- 1330 **Vislobokova I. 2004.** New species of *Orygotherium* (Palaeomerycidae, Ruminantia) from the
1331 Early and Late Miocene of Eurasia. *Annalen des Naturhistorischen Museums in Wien*
1332 **106**: 371–385.
- 1333 **Wang KM. 1929.** Die obermiozänen Rhinocerotiden von Bayern. *Paläontologische*
1334 *Zeitschrift*, **10**: 184–212.
- 1335 **Wang BY. 1965.** A new Miocene aceratheriine rhinoceros of Shanwang, Shandong.
1336 *Vertebrata Palasiatica* **9**: 109–112.
- 1337 **Zelenkov NV. 2016.** The first fossil parrot (Aves, Psittaciformes) from Siberia and its
1338 implications for the historical biogeography of Psittaciformes. *Biology Letters* **12**:
1339 20160717. DOI: 10.1098/rsbl.2016.0717
- 1340
- 1341 SUPPORTING INFORMATION

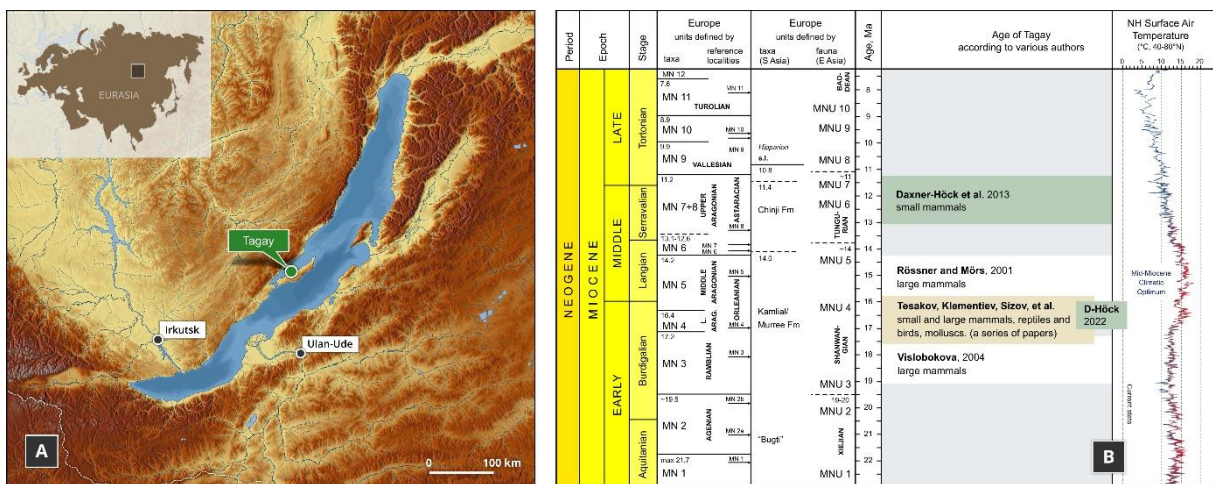
1342 Additional supporting information may be found online in the supporting information
 1343 tab for this article. Supplementary Files:

- 1344 • **S1.** Character matrix for the preliminary phylogenetic analysis, including 282 cranial,
 1345 dental, and postcranial characters controlled on 32 terminal taxa (one tapirid,
 1346 rhinocerotoids, and rhinocerotids), with Tagay rhinoceros and “Diaceratherium
 1347 shanwangense” as separate terminals.
- 1348 • **S2.** Output log text of the preliminary phylogenetic analysis (282 characters and 32
 1349 taxa).
- 1350 • **S3.** Character matrix for the final phylogenetic analysis, including 282 cranial, dental,
 1351 and postcranial characters controlled on 31 terminal taxa (one tapirid, rhinocerotoids,
 1352 and rhinocerotids).
- 1353 • **S4.** Output log text of the final phylogenetic analysis, with Bremer Support
- 1354 • **S5** Measurements for *Brachydiceratherium shanwangense* from Tagay site.

1355
 1356
 1357

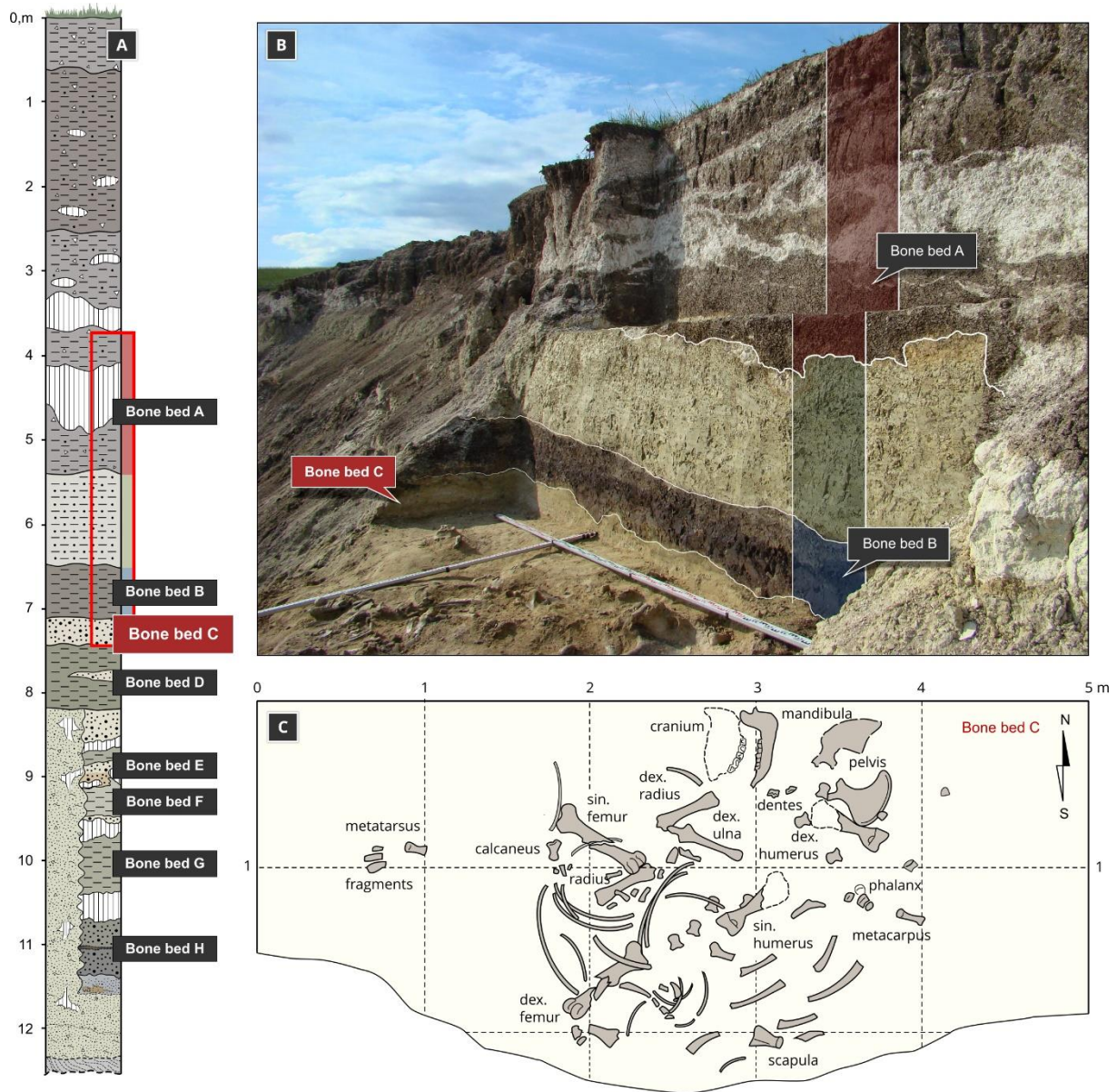
1358 FIGURES

1359



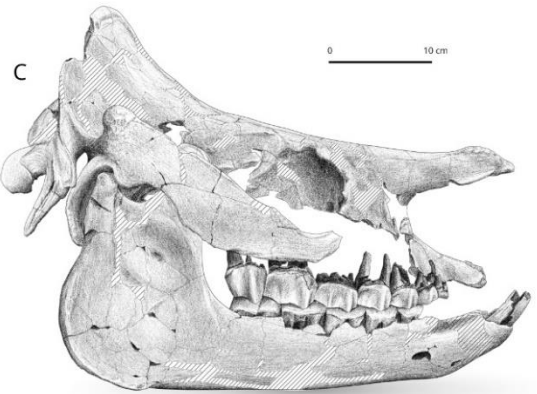
1360

1361 **Fig. 1.** Geographic position of Tagay locality on Olkhon Island, Baikal Region, Russia (A)
 1362 and age of Tagay Formation according to various authors (B). [Full width suggested]



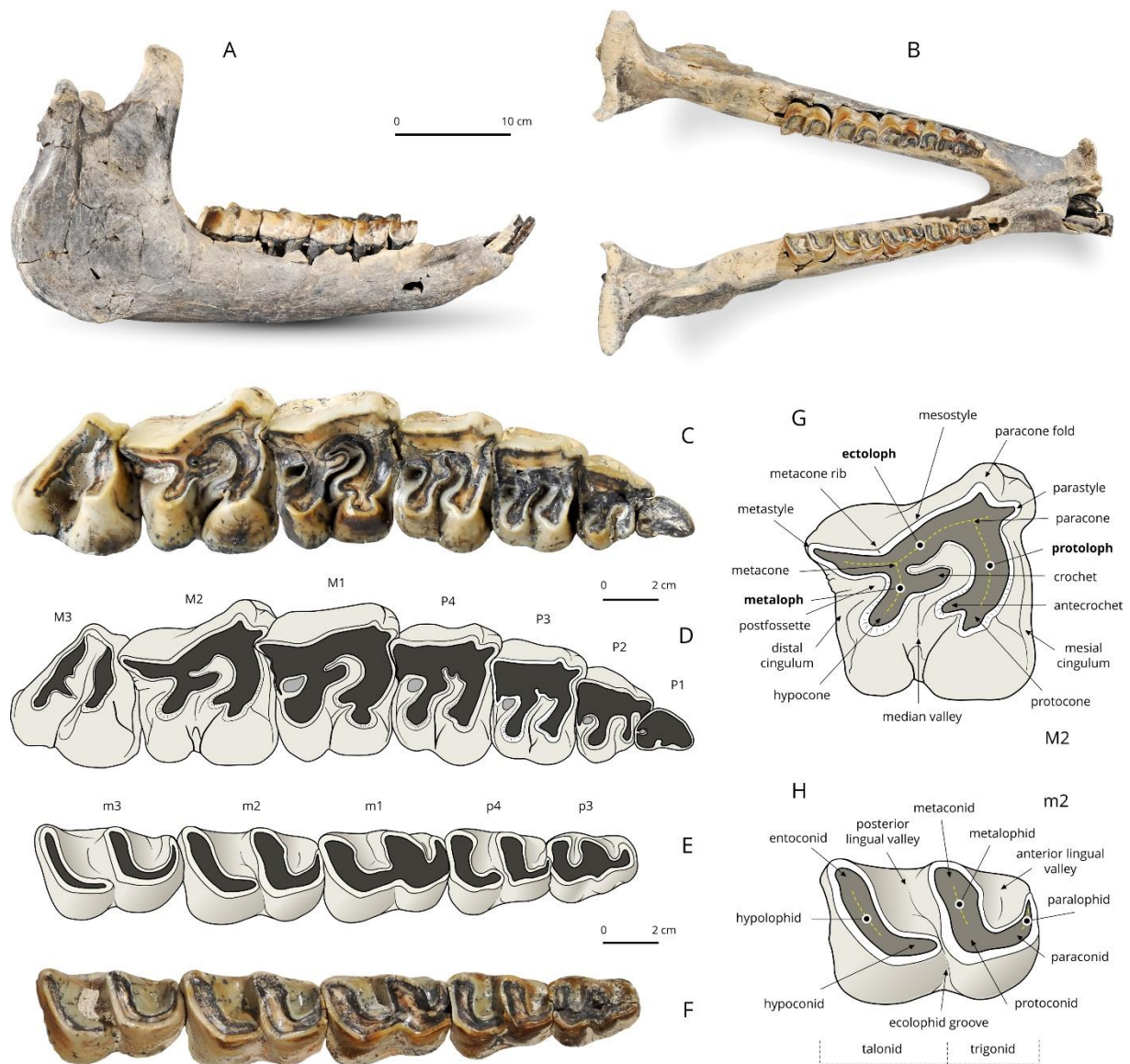
1363
 1364 **Fig. 2.** Geological structure of the Tagay section (A), photo (B) and plan (C) of the
 1365 excavations of the Miocene rhinocerotid at Tagay site in 2008 (Olkhon Island, Baikal Region,
 1366 Russia). [Full width suggested]

1367



1368

1369 **Fig. 3.** *Brachydiceratherium shanwangense* (Wang, 1965) from Tagay, Baikal Region,
1370 Russia, late early Miocene. Photos in dorsal (A) and lateral views (B) of the skull and
1371 mandible IZK79-1-08C-1. C - Scientific drawing of the right lateral view of the skull (based
1372 on B). Striped areas are reconstructed. D – Tentative reconstruction of the head in lateral
1373 view, by one of us (AS). [One column width suggested]



1374

1375 **Fig. 4.** *Brachydiceratherium shanwangense* (Wang, 1965) from Tagay, Baikal Region,

1376 Russia, late early Miocene. Mandible and dental material. A, B – Mandible in right lateral (A)

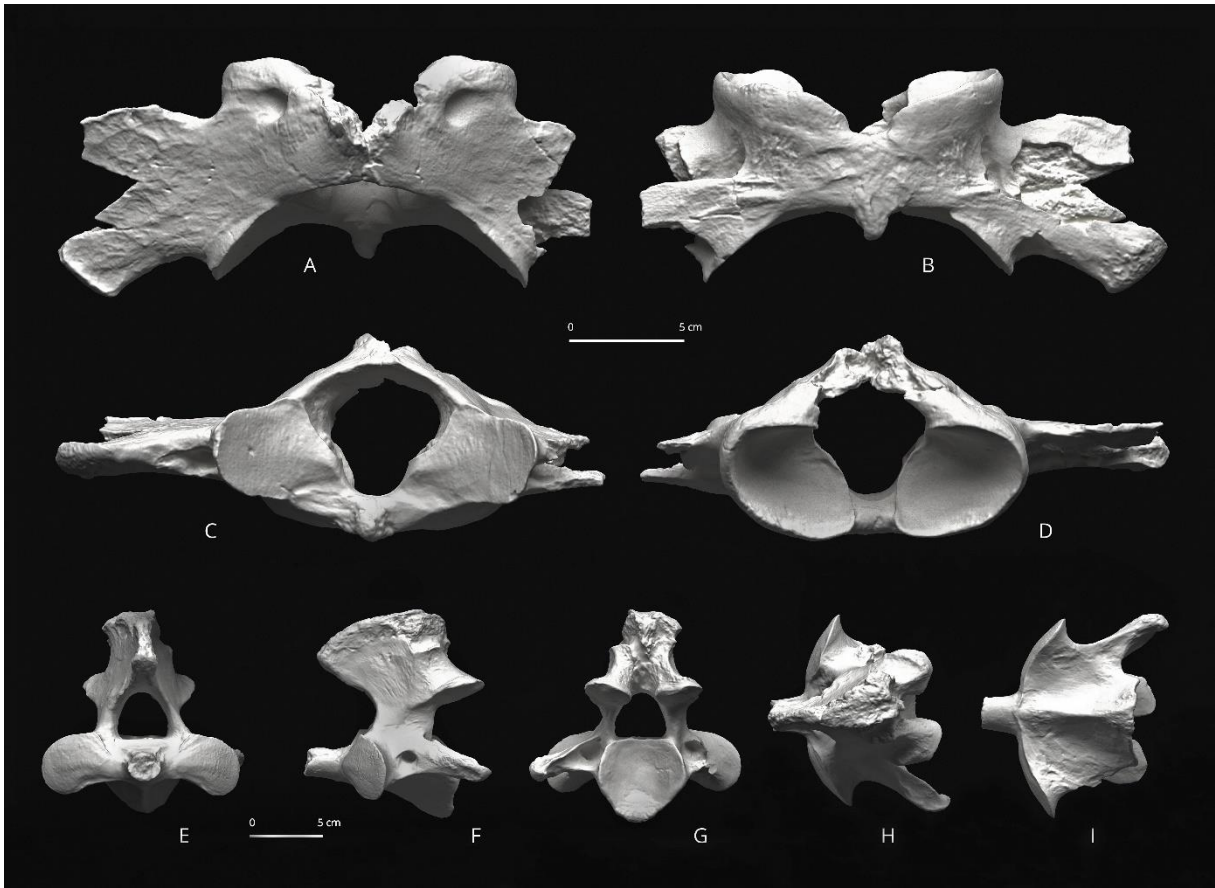
1377 and occlusal views (B); C, D – Right upper cheek teeth (D1–M3) in occlusal view:

1378 photograph (C) and interpretative sketch (D); E, F – Right lower cheek teeth (p3–m3) in

1379 occlusal view: photograph (E) and interpretative sketch (F); G, H – Dental terminology used

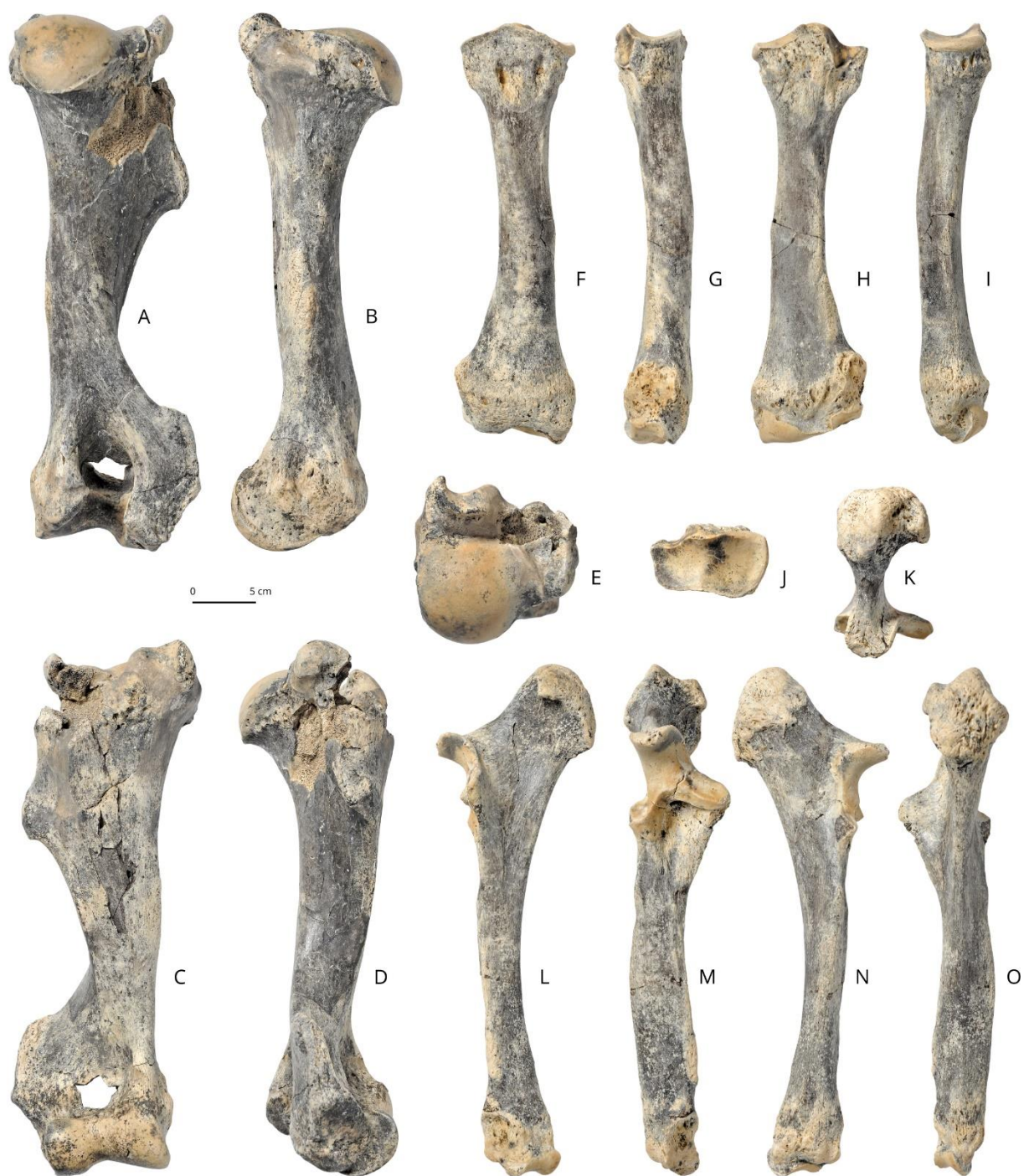
1380 for rhinocerotid upper tooth (G) and lower tooth (H). [Full width suggested]

1381



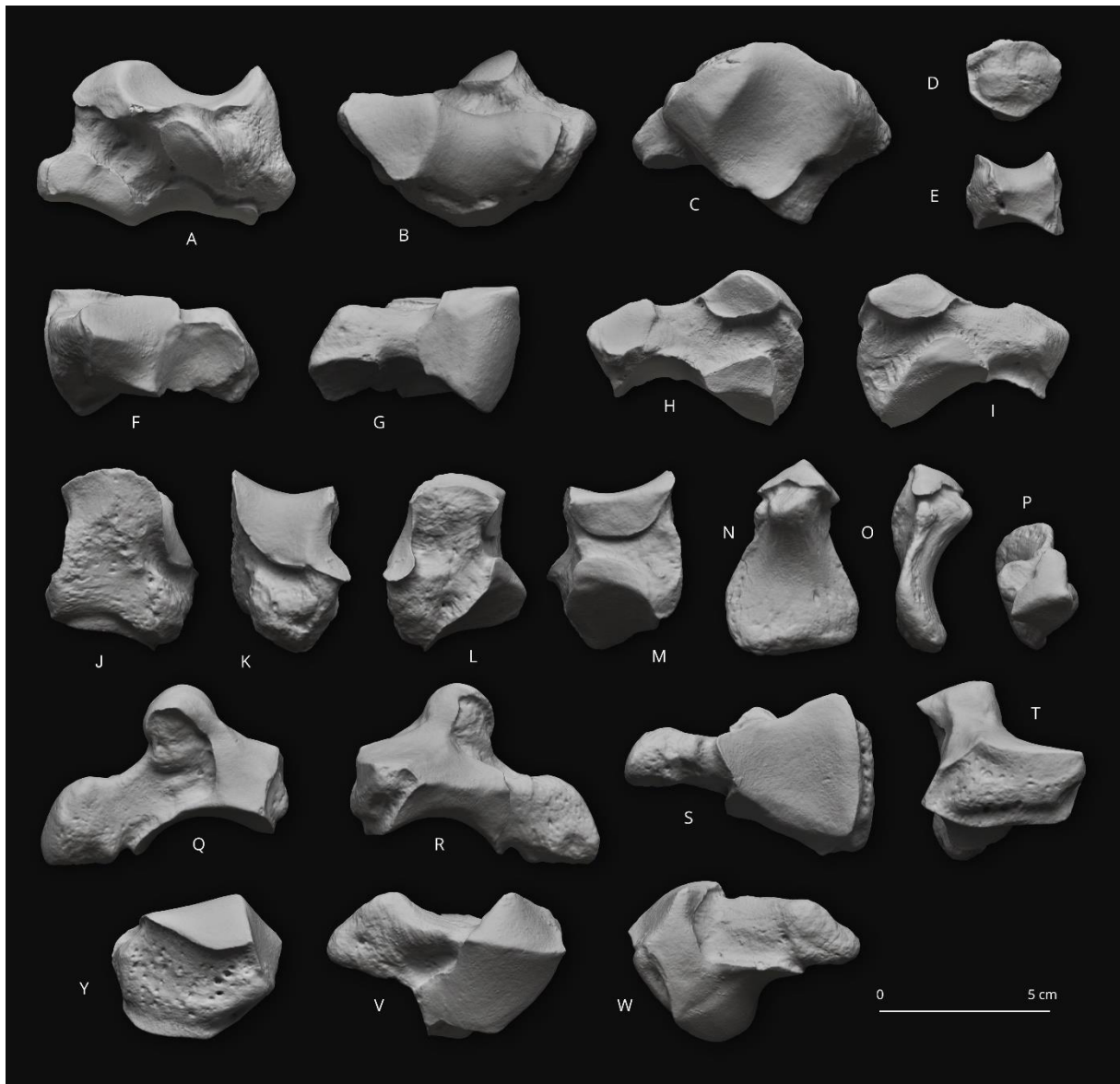
1382

1383 **Fig. 5.** *Brachydiceratherium shanwangense* (Wang, 1965) from Tagay, Baikal Region,
 1384 Russia, late early Miocene. A-D – Atlas in dorsal (A), ventral (B), cranial (C) and posterior
 1385 views (D); E-I – Axis in anterior (E), left lateral (F), posterior (G), dorsal (H), and ventral
 1386 views (I). [Full width suggested]



1387

1388 **Fig. 6.** *Brachydiceratherium shanwangense* (Wang, 1965) from Tagay, Baikal Region,
 1389 Russia, late early Miocene. Long bones of the right forelimb. A-E –humerus in posterior (A),
 1390 medial (B), anterior (C), lateral (D), and proximal views (E); F-J – radius in anterior (F),
 1391 lateral (G), posterior (H), medial (I), and proximal views (J); K-O – ulna in proximal (K),
 1392 medial (L), anterior (M), lateral (N), and posterior views (O). [Full width suggested]



1393

1394 **Fig. 7.** *Brachydiceratherium shanwangense* (Wang, 1965) from Tagay, Baikal Region,
 1395 Russia, late early Miocene. Carpal bones. A-C – left scaphoid in posterior (A), proximal (B),
 1396 and distal views (C); D-E – right trapezoid in anterior (D), and distal views (E); F-I – left
 1397 semilunate in distal (F), proximal (G), medial (H), and lateral views (I); J-M – left pyramidal
 1398 in anterior (J), lateral (K), posterior (L), and medial views (M); N-P – right pisiform in
 1399 anterior (N), lateral (O), and proximal views (P); Q-T – right magnum in lateral (Q), medial
 1400 (R), distal (S), and anterior views (T); Y-W – right unciform in anterior (Y), proximal (V),
 1401 and distal (W). [Full width suggested]



1402

1403 **Fig. 8.** *Brachydiceratherium shanwangense* (Wang, 1965) from Tagay, Baikal Region,
 1404 Russia, late early Miocene. Left metacarpal bones. A-E – second metacarpal in lateral (A),
 1405 posterior (B), medial (C), anterior (D), and proximal views (E); F-J – third metacarpal in
 1406 proximal (F), lateral (G), posterior (H), medial (I), and anterior views (J); K-O – fourth
 1407 metacarpal in proximal (K), lateral (L), posterior (M), medial (N), and anterior views (O).

1408 [Full width suggested]

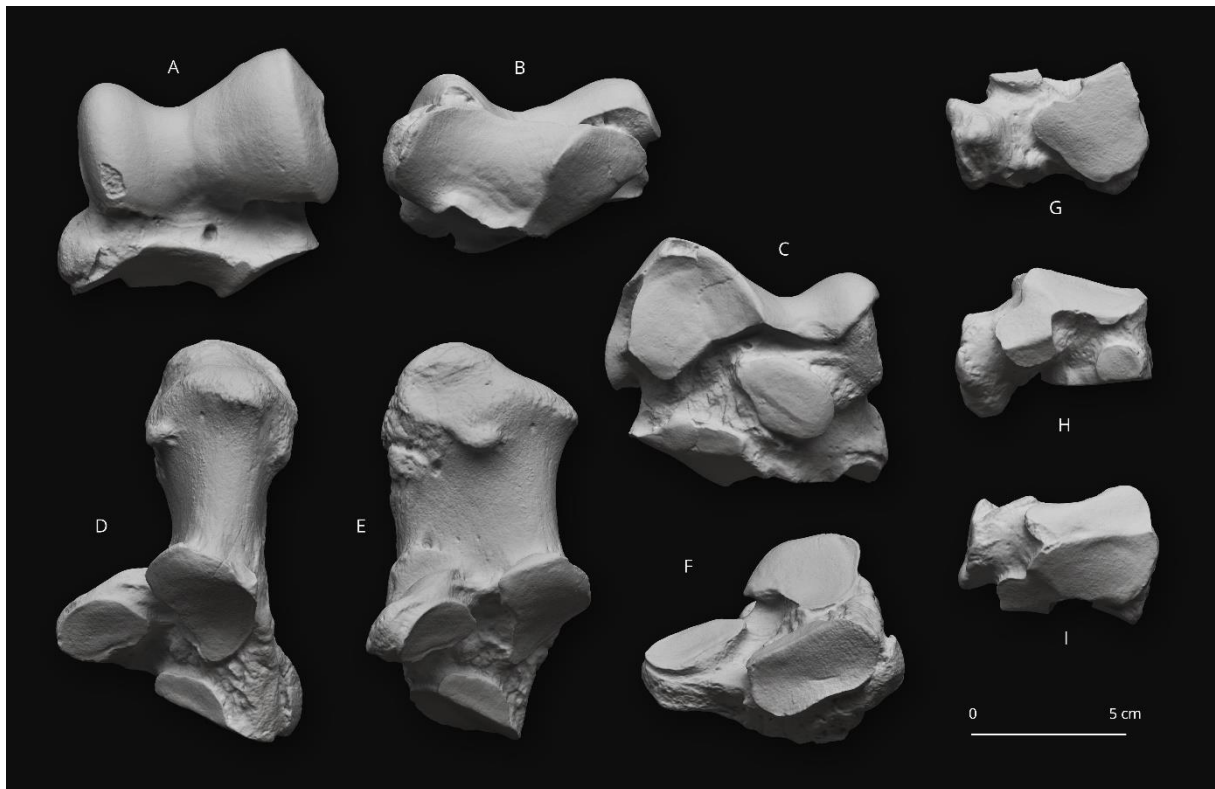
1409

1410



1411

1412 **Fig. 9.** *Brachydiceratherium shanwangense* (Wang, 1965) from Tagay, Baikal Region,
 1413 Russia, late early Miocene. Long bones of the left hind limb. A-F – femur in anterior (A),
 1414 medial (B), posterior (C), lateral (D), proximal (E), and distal views (F); G-J – fibula in lateral
 1415 (G), posterior (H), medial (I), and anterior views (J); K-O – tibia in anterior (K), medial (L),
 1416 posterior (M), lateral (N), and proximal views (O). [Full width suggested]



1417

1418 **Fig. 10.** *Brachydiceratherium shanwangense* (Wang, 1965) from Tagay, Baikal Region,
1419 Russia, late early Miocene. Tarsal bones. A-C – left astragalus in anterior (A), distal (B), and
1420 posterior views (C); D-F – left calcaneus in proximal (D), medial (E), and anterior views (F);
1421 G-I – left cuboid in distal (G), lateral (H), and proximal views (I). [Full width suggested]

1422

1423

1424



1425

1426 **Fig. 11.** *Brachydiceratherium shanwangense* (Wang, 1965) from Tagay, Baikal Region,
1427 Russia, late early Miocene. Metatarsal bones. A-E – left second metatarsal in lateral (A),
1428 posterior (B), medial (C), anterior (D), and proximal views (E); F-J – right fourth metatarsal
1429 in proximal (F), medial (G), posterior (H), lateral (I), and anterior views (J). [Full width
1430 suggested]

1431

1432

1433

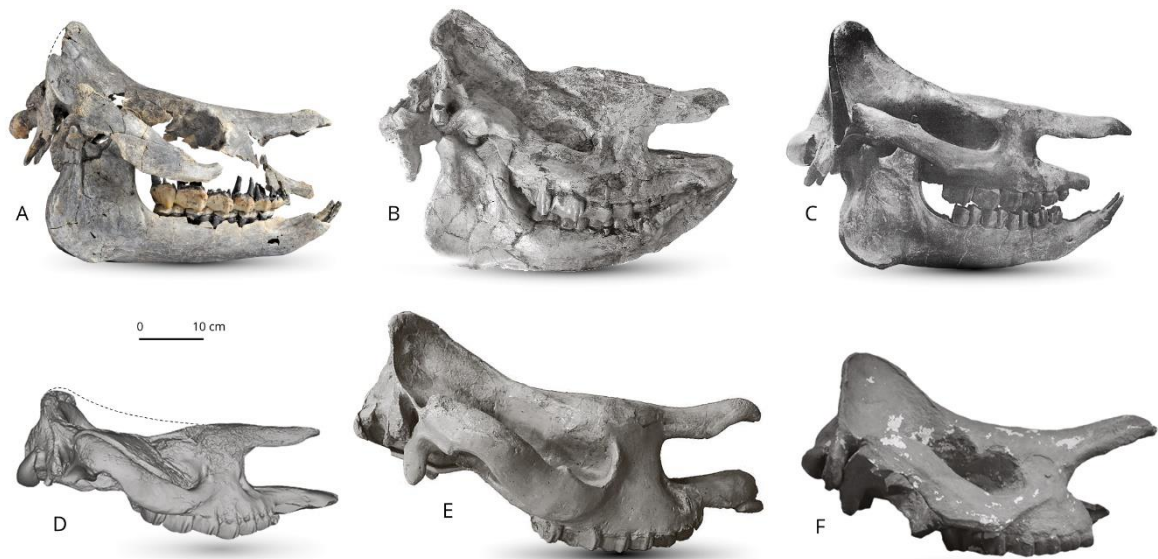
1434

1435

1436

1437

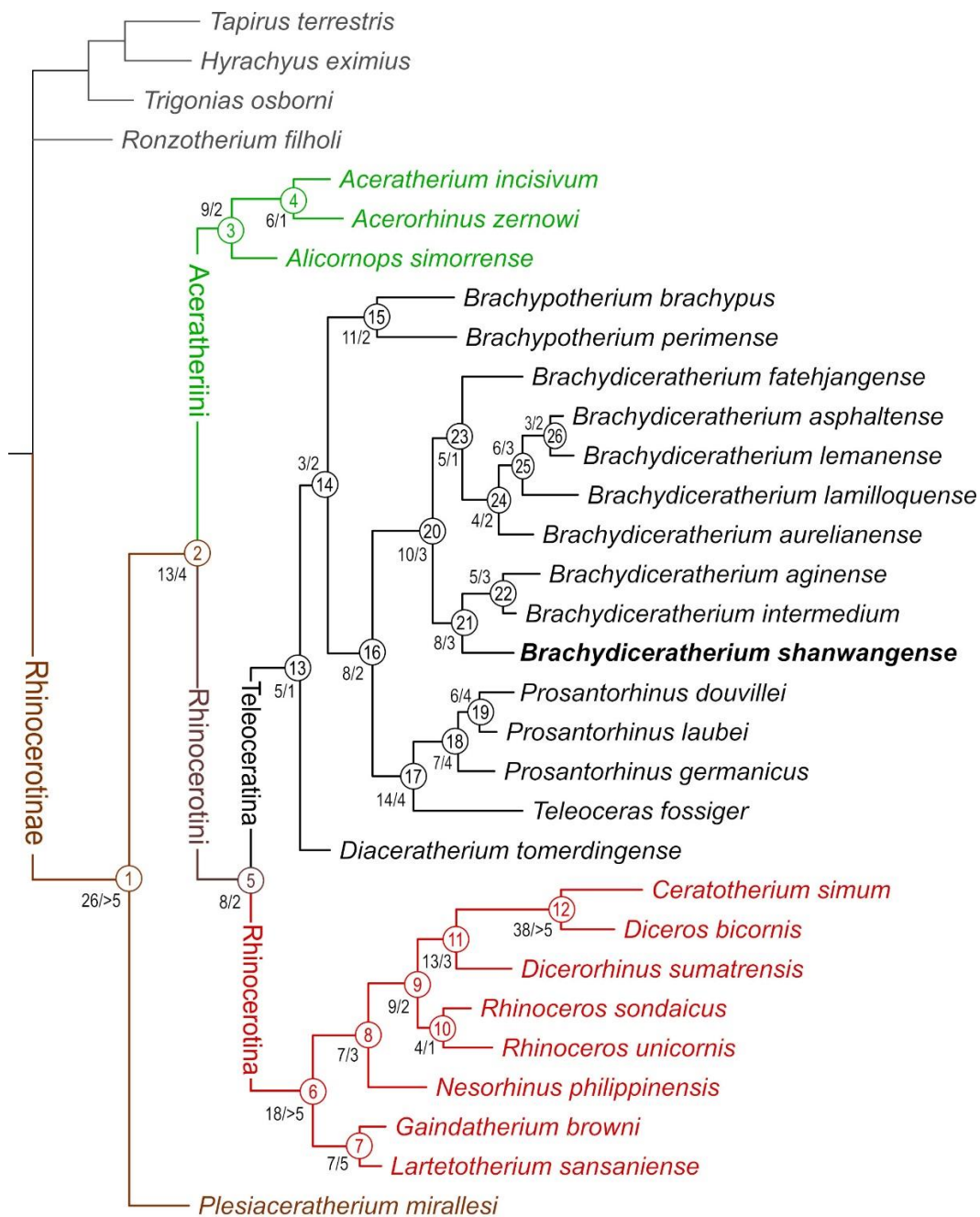
1438



1439

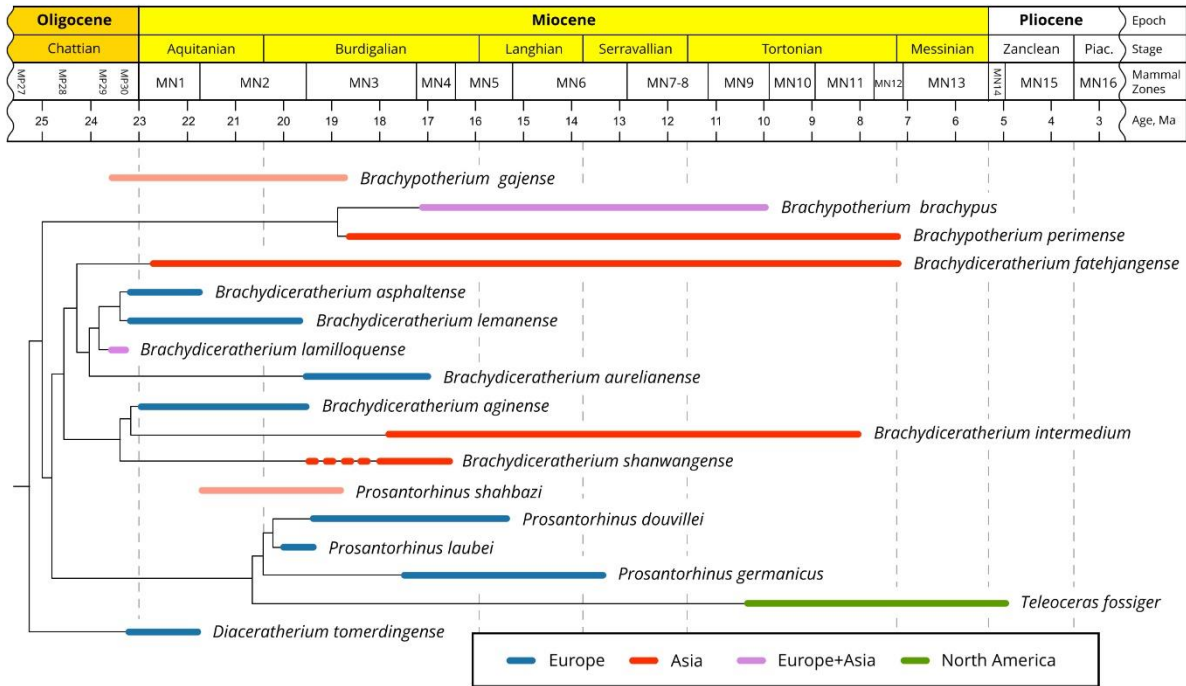
1440 **Fig. 12.** Skulls of different species of *Brachydiceratherium* in right lateral view. **A** -
1441 *Brachydiceratherium shanwangense* from Tagay (Baikal Region, Russia, late early Miocene)
1442 №IZK79-1-08C-1/1; **B** - *Brachydiceratherium shanwangense* from Jijiazhuang locality STM
1443 44–98 (deformed, mirrored) (MN4 - early Miocene, Shanwang Basin, Shandong Province,
1444 China) №MHNT.PAL.2013.0.1001; **C** - *Brachydiceratherium aginense* (Répelin, 1917) from
1445 Laugnac (MN2 - early Miocene, Lot-et-Garonne, France); **D** - *Brachydiceratherium*
1446 *lemanense* from Gannat (MN1 - early Miocene, France) №MNHN-AC-2375, holotype; **E** -
1447 *Brachydiceratherium asphaltense* (Depéret et Douxami, 1902) from Saulcet (MN1 - earliest
1448 Miocene, Allier, France). №NMB–Sau1662; **F** - *Brachydiceratherium aurelianense* from
1449 Neuville-aux-Bois (MN3 - early Miocene, France) №MHNT.PAL.2013.0.1001, cast of the
1450 holotype; [Full width suggested]

1451



1452 — 10 changes

1453 **Fig. 13.** Phylogram of Rhinocerotinae, with a focus on Teleoceratina. Most parsimonious tree
 1454 (1316 steps; consistency index = 0.2698; retention index = 0.4918), retrieved from 282
 1455 unweighted cranio-mandibular, dental, and postcranial characters scored in 31 tapirid and
 1456 rhinocerotoid species (see S3 and S4). Node numbers appear in empty circles. Number of
 1457 unambiguous synapomorphies/Bremer Support are indicated left to nodes. [Full width
 1458 suggested]



1459

1460 **Fig. 14.** Phylogenetic relationships of Teleoceratina versus time (see Fig. 13), with new
 1461 combinations. Although they were not included in the current parsimony analysis, the
 1462 temporal distributions of *Brachypotherium gajense* and *Prosantorhinus shahbazi* are provided
 1463 here, as these species might bridge a stratigraphic gap for the concerned genera. Red dotted
 1464 line for *B. shanwangense* stands for the age uncertainty of Tagay locality (MN3-5) [Full width
 1465 suggested]

1466



1467

1468

Fig. 15. Paleomap of Eurasia by early Miocene times (~20 Ma), showing the main

1469

occurrences of representatives of the teleoceratine rhinocerotid *Brachydiceratherium*, at the

1470

basin scale (apart from Tagay, Shanwang, and Nong Ya Plong localities). The Green area

1471

depicts the interpolated geographical range of *B. shanwangense* (with possible occurrences on

1472

Honshu Island, Japan). Based on data from Borissiak (1927), Cerdeño (1993), Antoine et al.

1473

(2000, 2013), Becker et al. (2009), Antoine & Becker (2013), Tomida et al. (2013), Jame et

1474

al. (2019), Handa (2020), Lu et al. (2021), Antoine (in press), and the present work.

1475

PalaeoAtlas by Scotese (2016, under cc 4.0 license) with added paleomap for the Baikal area

1476

(Mats et al., 2011). [Full width suggested]

1477

1478

1479

1480

1481

1482 **Table 1.** Cranial measurements of *Brachydiceratherium shanwangense*, from Tagay, early
 1483 Miocene of Eastern Siberia, in mm. 1, Length (occipital-premaxilla distance); 2, Length
 1484 (occipital-nasal distance); 3, Upper length (nasal-occipital crest distance); 4, Nasal incisure
 1485 length; 5, Minimal width; 6, Occipital crest-postorbital process distance; 8, Occipital crest-
 1486 lacrimal process distance; 9, Nasal incisure-orbit distance; 13, Post-M3-condyle distance; 14,
 1487 Nasal-orbit distance; 15, Occipital crest width; 16, Mastoid apophyses width; 17, Inter
 1488 frontoparietal crest minimal distance; 18, Postorbital process width; 19, Lacrimal process
 1489 width; 21, Zygomatic width; 22, Nasal incisure width; 23, Occipital height; 25, P2-level
 1490 height; 26, P4-M1-level height; 27, M3-level height; 31, Foramen magnum width; 32, Inter-
 1491 occipital condyle width. Numbers coincide with measurements as defined and illustrated by
 1492 Guérin (1980, fig. 1, table 1).

1	2	3	4	5	6	8	9	13	14	15	16
505	540	455.8	(174)	125	249.6	293.6	(72.6)	(254)	219	(160)	224.8
17	18	19	21	22	23	25	26	27	31	32	
26.7	179	189	308.2	69.7	144.6	(140)	(155)	(156)	43	112.4	

1500
 1501

1502 **Table 2.** Right mandibular measurements of *Brachydiceratherium shanwangense*, from
 1503 Tagay, early Miocene of Eastern Siberia, in mm. 1, Maximal length; 2, Length without the
 1504 symphysis; 3–8, Heights of the corpus mandibulae, between p2-p3, p3-p4, p4-m1, m1-m2,
 1505 m2-m3, and behind m3, respectively; 9 and 10, Transverse diameters of the corpus
 1506 mandibulae, between p4-m1 and behind m3, respectively; 11, Antero-posterior length of the
 1507 symphysis; 13, Antero-posterior diameter of the ramus (at the level of the occlusal line); 14,
 1508 Transverse diameter of the articular condyle; 15, Height of the articular condyle; 16, Height
 1509 of the coronoid process. Numbers coincide with measurements as defined and illustrated by
 1510 Guérin (1980, fig. 1, table 3).

1511

1	2	3	4	5	6	7	8	9	10	11	13	14	15	16
467.4	136.8	68	68	70.7	75	76.4	77.7	38.1	41.3	118.2	136.8	96.2	203.3	229.2

1512

1513

1514 **Table 3.** Dental measurements of *Brachydiceratherium shanwangense*, from Tagay, early
 1515 Miocene of Eastern Siberia, in mm. Abbreviations: H, crown height; L, length; W, width.
 1516

		P1	P2	P3	P4	M1	M2	M3	p2	p3	p4	m1	m2	m3
left	L		c25.1	31.5	35.3	47.0	50.5			28.0	31.8	38.6	43.8	43.9
	W		31.5	41.1	47.7	51.7	54.2			21.8	25.2	27.6	29.8	30.5
	H		17.1	21.7	28.3	30.5	37.5			18.2	23.2	28.8	30.2	29.8
right	L	19.3	27.2	29.0	35.5	47.1	50.6	42.1		29.8	32.0	37.7	44.1	45.4
	W	14.5	31.9	40.0	47.6	51.4	56.2	46.1		21.9	27.2	28.1	30.0	30.3
	H	8.8	18.0	21.1	27.0	29.7	37.6	37.8		19.8	23.0	24.8	28.7	27.0

1517

1518 **Table 4.** Postcranial measurements of *Brachydiceratherium shanwangense*, from Tagay, early
 1519 Miocene of Eastern Siberia, in mm. Forelimb bones. Abbreviations: ant, anterior; APD,
 1520 antero-posterior diameter; art, articulation; artic, articular; D, distance; del, deltoid; dist,
 1521 distal; ext, extremity; H, height; L, length; lat, lateral; mag, magnum; max, maximal; med,
 1522 medial; mid, middle; post, posterior; pyr, pyramidal; rad, radius; sml, semilunate; TD,
 1523 transverse diameter; tpz, trapezium; tpzd, trapezoid; troch, trochlea; tub, tuberosity; unc,
 1524 unciform.

Scapula	-	-	-	-	-	-	glenoid cavity		-	-	-	-	-	
							TD	APD						
							65	86.8						
Humerus	L	proximal ext		diaphysis		dist		TD	TD	APD trochlea				
	400.3	TD	APD	TD	APD	TD	APD	del	tub	104	troch	med	mid	lat
		120.7	126.8	54.1	55.1	127.6	99				92.5	75	42	57.2
Radius	max L	proximal ext		proximal art		diaphysis		distal extremity		distal articulation		-		
	324.1	TD	APD	TD	max APD	TD	APD	TD	APD	TD	APD	TD	APD	-
		88.1	58	87	47.7	39	36.5	95.5	54.4	84.6	40			
Ulna	artic L	olecranon		humeral cochlea		diaphysis		pyramidal-facet		dist radius-facet		-		
	353.9	TD	H	TD	H	TD	APD	46.3	TD	APD	APD	H		
		67.5	79.8	81.3	66.5	31.4		32.1	46.5	16.5	7.2			
Scaphoid	ant H	post H	TD	APD	rad-fac	tpz-fac		trap-fac		mag-fac		-		
	49	46.4	52.7	73.6	APD 39	TD	APD	TD	APD	TD	APD	TD	APD	-
						18.6	12.4	29.1	39.7	30.4	31.3			
Semilunate	TD	APD	H	post TD	mag-facet		unc-facet		scaph-fac D		pyram-fac D		-	
	36.1	63.6	47.1	28.1	TD	APD	TD	APD	17.8	33	10.7	6.3		
					22.8	47.7								
Pyramidal	TD	APD	ant H	56.5	ul-fac	unciform-facet		semilunate-facet		-		-		
	45.3	44			APD	TD	APD	D	prox H	dist H				
					32.6	38.9	28.5	6.8	12.7	9.5				
Pisiform	TD	APD	tuberosity	ulna-fac	pyr-fac	-		-		-		-		
	57.7	26.4	H	APD	TD	TD								
			40.9	15.1	18.6	18.9								
Trapezoid	TD	APD	ant H	mid H	post H	-		-		-		-		
	34.4	35	27.6	19.6	29.4									
Magnum	TD 49	ant H	H	APD	sml-fac	McIII-facet		post tuberosity		-		-		
		26.1	47.7	74.1	APD 40.2	TD	APD	TD	H	17.6	25.9			
						43.5	42.2							
Unciform	TD	H 40.1	APD		post tuberosity		semilunate-fac		pyramidal-facet		McV-fac			
	52.8		max	min	TD	H	TD	APD	TD	APD	TD	APD		
			71.7	56.9	31	20.7	22.2	36.8	33.8	40.7	23.1	29.6		
McII	L	TD	proximal art		trapezoid-facet		TD		diaphysis		dist articulation		-	
	130.9	41	TD	APD	TD	APD	TD	APD	TD	APD	TD	APD		
			41	37.3	30.6	36.4	37.3	17.1	40.4	41.9				
McIII	L	med L	proximal art		McIV-facets	magnum-facet		diaphysis		dist ext		distal art		
	143.2	133.2	TD	APD	D	TD	APD	TD	APD	TD	TD	TD	APD	
			55.9	40.7	12.3	43.5	41.5	44	19.4	54.4	44.5	41		
McIV	L	proximal art		unciform-facet		McV-facet		diaphysis		dist ext		distal art		
	114.7	TD	APD	TD	APD	H	APD	TD	APD	TD	TD	TD	APD	
		38.1	40.2	29.1	39.6	12.7	15.3	32.8	16.8	43.2	35.1	36.3		
McV	L	TD	APD 25.7		McIV-facet		unc-fac		-		-		-	
	20	27.2			H	APD	APD							
					12.9	19	22.9							

1526
 1527
 1528
 1529

1530 **Table 5.** Postcranial measurements of *Brachydiceratherium shanwangense*, from Tagay, early
 1531 Miocene of Eastern Siberia, in mm. Hind limb bones. Abbreviations: ant, anterior; APD,
 1532 antero-posterior diameter; art, articulation; artic, articular; As3, astragalus-3 (sensu Heissig,
 1533 1972); astr, astragalus; Cc1, calcaneus-1 (sensu Heissig, 1972); Cc2, calcaneus-2 (sensu
 1534 Heissig, 1972); D, distance; dist, distal; ext, extremity; H, height; L, length; lat, lateral; maj,
 1535 major; max, maximal; med, medial; mesocun, mesocuneiform; mid, middle; min, minimum;
 1536 post, posterior; sust, sustentaculum; TD, transverse diameter; tr, trochanter; troch, trochlea;
 1537 tuber, tuberosity.

Femur	L 486.9	proximal ext		maj tr		third tr		diaphysis		dist ext		distal condyles	
		TD	APD	TD	TD	H	TD	APD	TD	APD	TD	D	
		164.2	72.4	97	54.5	51.6	63.5	43	129.4	144.8	114.3	10.7	
Patella	TD	APD	H	articulation		med lip		lateral lip		-	-	-	-
	80.1	34	84	TD	H	TD	TD	H	TD	H			
				68.3	82.5	53.5	29.2	69.5					
Tibia	L	proximal ext		diaphysis		dist ext		fibula-facet		astr cochlea		-	
	333	TD	APD	TD	APD	TD	APD	APD	H	TD	APD		
		115.3	100.5	47	40.5	89.5	60.6	33.6	9.7	70.6	50.1		
Fibula	L	proximal ext		diaphysis		dist ext		tibia-facet		astr facet		-	
	267.7	TD	APD	TD	APD	TD	APD	APD	H	APD	H		
		25	39.3	47	40.5	11.8	14.4	37.1	9.6	37.1	18.7		
Astragalus	max	troch	max	H			Cc1-facet		Cc2-facet		cuboid-facet		
	TD	TD	APD	medial	mid	lateral	TD	H	TD	H	L	W	
	90.9	75.1	53.4	67.3	52.3	70.5	40.5	37.6	39.5	22.5	45	23.2	
Calcaneus	H	artic	tuberosity	beak	sust TD	tuber min	As3-facet		cuboid-facet		-		
	128.9	H 67.3	TD	APD	APD	73.7	TD	APD	TD	H	TD	H	
			46.8	61.8	62.9		28.8	51	30.1	11.4	43.9	20.4	
Cuboid	TD	max		H		proximal art		distal art		-	-	-	
	ant	post	APD	ant	post	TD	APD	TD	APD				
	43	31	61.9	29.9	49.4	39.6	43.8	37.3	37.1				
MtII	L	proximal art		mesocun-fac		lat facet H		diaphysis		distal art		-	
	160	TD	APD	TD	APD	ant	post	TD	APD	TD	APD		
		31.3	39.9	25.4	28.4	5.4	12.9	28.7	19.4	33.8	39.5		
MtIV	L 101.7	proximal art		medial facets				diaphysis		dist ext		distal art	
		TD	APD	ant TD	ant H	post TD	post H	TD	APD	max TD	TD	APD	
		31.7	33.3	11.3	16.9	18.7	14.8	30.5	18.1	38.3	30.4	40.2	

1539

1540

1541 **Table 6.** Distribution of unambiguous apomorphic characters (synapomorphies and
1542 autapomorphies, including reversals) among teleoceratine rhinocerotids, as retrieved in the
1543 current phylogenetic analysis. Node numbers match those of Fig. 13. Binominal combinations
1544 are as detailed in the Discussion.

1545 Node 13 (Teleoceratina): -72⁰, 129¹, 205¹, 279¹, 282¹

1546 *Diaceratherium tomerdingense* (type and only species): -70⁰, 90¹, 121¹, 130¹, -196⁰, 212¹,
1547 216¹, 223³, 228², -251⁰

1548 Node 14: 199², 202¹, 227¹

1549 *Brachypotherium*: -50⁰, 54², -83¹, -114⁰, 140¹, -146⁰, 155¹, 203¹, 214¹, -226⁰, 254¹

1550 *Brachypotherium brachypus*: 3², -34⁰, -39⁰, 57¹, 62¹, 99², -109¹, -115², 118¹, -119⁰, -135⁰,
1551 144¹, -149⁰, 157³, -159⁰, -160⁰, 170¹, 179¹, 180¹, 191¹, -193⁰, -204⁰, 209¹, 210¹, 239¹, 275², -
1552 -280⁰

1553 *Brachypotherium perimense*: 25¹, 41¹, 68¹, 76¹, -85⁰, 121¹, -125⁰, 128¹, -129⁰, 151³, 172¹,
1554 173¹, 175¹, 181¹, 199³, 200¹, -205⁰, 228², 246¹, 248¹, 255¹, 263³, -271⁰, 272¹, 274¹, 277¹, -
1555 282⁰

1556 Node 16: 38¹, 101¹, 107³, -147⁰, -222⁰, -230⁰, -263⁰, 264³

1557 Node 17 (*Teleoceras* + *Prosantorhinus*): 10¹, 11¹, 40¹, 57¹, 95¹, 99¹, 130¹, 180¹, 190², 191¹,
1558 234¹, 272², 275², -280⁰

1559 *Teleoceras fossiger* (type species): 2¹, 19¹, 25¹, 48¹, -56⁰, 59¹, 60⁰, 63¹, 68¹, 80¹, 87², 88², 91²,
1560 99², 102¹, 114³, 116¹, 117¹, 121¹, 126¹, 128¹, 144¹, 151³, 153¹, 157³, 159³, 165¹, 173¹, 175¹,
1561 180³, -196⁰, 212¹, 220¹, 248¹, -249⁰, 254¹, 268¹, 269¹, 276¹

1562 *Prosantorhinus*: 1¹, 27¹, -35⁰, 45¹, -119⁰, -125⁰, -177⁰

1563 *Prosantorhinus germanicus* (type species): 37¹, 85³, 105¹, -109¹, -110⁰, -111², 115², 147²,
1564 148¹, -149¹, -151¹, 166¹, -182⁰

1565 Node 19: -101⁰, -129⁰, -135⁰, -159¹, 182², 261³

- 1566 *Prosantorhinus laubei*: -85¹, 90¹, -99⁰, -114⁰, -134⁰, -180⁰
- 1567 *Prosantorhinus douvillei*: -88⁰, 99², 114², 144¹, 156², -157⁰, -159⁰, 162¹, 180³
- 1568 *Brachydiceratherium*: -20⁰, -39⁰, 65¹, 101³, -149¹, -159⁰, 185¹, 187², 246¹, -251⁰
- 1569 Node 21: 72¹, 105², -190⁰, -193⁰, 238¹, 250¹, -279⁰, -282⁰
- 1570 *Brachydiceratherium shanwangense*: 1¹, 27¹, 63¹, -70⁰, -85⁰, 87², 88², 105³, 116¹, 147², 151³,
- 1571 157³, 191¹, -196⁰, 199³, 234¹
- 1572 Node 22: 121¹, 210¹, -252¹, -264⁰, -265⁰
- 1573 *Brachydiceratherium aginense*: 112¹, -114⁰, 128², 130¹, -149⁰, 162¹, 214¹, 216¹, 219¹, -221⁰, -
- 1574 226⁰, 256¹, -262⁰, 263¹, 272¹, -280⁰
- 1575 *Brachydiceratherium intermedium*: -65⁰, 114³, 118¹, -129⁰, 220¹
- 1576 Node 23: -119⁰, 203¹, -204⁰, 207¹, 261¹
- 1577 *Brachydiceratherium fatehjangense*: 10¹, 18², 48¹, -49⁰, 53¹, 54², 57¹, -70⁰, -94¹, -107⁰, 140¹, -
- 1578 149⁰, 151³, 155¹, 174¹, -202⁰, -205⁰, 209¹, -224⁰, -227⁰, -247⁰, 261²
- 1579 Node 24: 118¹, -125⁰, -134⁰, 230¹
- 1580 *Brachydiceratherium aurelianense*: -53⁰, 86¹, 90³, 114³, 124¹, 130¹, 147¹, -193⁰, 198¹, -199⁰,
- 1581 214¹, 220¹
- 1582 Node 25: 105¹, 210¹, -253⁰, -264⁰, -279⁰, -280⁰
- 1583 *Brachydiceratherium lamilloquense*: 53², -84¹, 88¹, 99¹, -102¹, 105³, -111², 112³, -135⁰, -146⁰,
- 1584 207², 228², -243⁰, -246⁰, -247⁰, 248¹, -259⁰
- 1585 Node 26: -109⁰, -138⁰, -221⁰
- 1586 *Brachydiceratherium asphaltense*: -23⁰, 27¹, 83³, -227⁰
- 1587 *Brachydiceratherium lemanense* (type species): 11¹, 40¹, 45¹, -47⁰, 48¹, -50⁰, -70⁰, 147¹, -226¹
- 1588
- 1589
- 1590